Light distribution and spectral composition within cultures of micro-algae: Quantitative modelling of the light field in photobioreactors

David Fuente[1,*], Joseph Keller[2], J. Alberto Conejero[3], Matthias Rögner[2], Sascha Rexroth[2], and Javier F. Urchueguía[1]

[1]Instituto de Aplicaciones de las Tecnologías de la Información y de las Comunicaciones Avanzadas, Universitat Politècnica de València, València, Spain

[2]Plant Biochemistry, Faculty of Biology and Biotechnology, Ruhr University Bochum, Germany

[3]Instituto Universitario de Matemática Pura y Aplicada, Universitat Politècnica de València, Valencia, Spain

[*]Corresponding author: dafueher@upv.es

January 11, 2017

Abstract

Light, being the fundamental energy source to sustain life on Earth, is the external factor with the strongest impact on photosynthetic microorganisms. Moreover, when considering biotechnological applications such as the production of energy carriers and commodities in photobioreactors, light supply within the reactor volume is one of the main limiting factors for an efficient system. Thus, the prediction of light availability and its spectral distribution is of fundamental importance for the productivity of photo-biological processes.

The light field model here presented is able to predict the intensity and spectral distribution of light throughout the reactor volume based on the incident light and the spectral characteristics of the photosynthetic microorganism. It takes into account the scattering and absorption behaviour of the micro-algae, as well the adaptation of the biological system to different light intensities.

Although in the form exposed here the model is optimized for photosynthetic microorganism cultures inside flat-type photobioreactors, the theoretical framework is easily extensible to other geometries. Our calculation scheme has been applied to model the light field inside Synechocystis sp. PCC 6803 wild-type and Olive antenna mutant cultures at different cell-density concentrations exposed to white, blue, green and red LED lamps, delivering results with reasonable accuracy, despite the data uncertainties. To achieve this, Synechocystis experimental attenuation profiles for different light sources were estimated by means of the Beer-Lambert law, whereby the corresponding downward irradiance attenuation coefficients $K_d(\lambda)$ were obtained through inherent optical properties of each organism at any wavelength within the photosynthetically active radiation band. The input data for the algorithm are chlorophyll-specific absorption and scattering spectra at different mean acclimatisation irradiance values for a given organism, the depth of the photobioreactor, the cell-density and also the intensity and emission spectrum of the light source.

In summary, the model is a general tool to predict light availability inside photosynthetic microorganism cultures and to optimize light supply, in respect to both intensity and spectral distribution, in technological applications. This knowledge is crucial for industrial-scale optimisation of light distribution within photobioreactors and is also a fundamental parameter for unravelling the nature of many photosynthetic processes.

Keywords: absorption, scattering, attenuation, inherent optical properties, modelling, Synechocystis

1 Introduction

1.1 Light research in aquatic ecosystems

1.1.1 Introduction to Optics in Biology

Photosynthesis is a very active research field in the life sciences due to the crucial importance of photosynthetic organisms as the fundamental source of all biomass in our planet. Particularly, much research has been done in understanding how light behaves inside different water bodies, such as inland, coastal and oceanic ecosystems.

Concurrently, bio-optical researchers have developed several methodologies to estimate optical properties. In the year 1961 Preisendorfer defined the inherent (IOPs) and apparent optical properties (AOPs) of water bodies, founding optical oceanography [1]. Relating IOPs and AOPs have been an ongoing effort since then, and different authors have studied, experimentally as well as theoretically [2], the optical characteristics of water and cell suspensions as a function of water body features and metabolic variables such as the energy stored by algae upon light conditions [3].

But oceanic optics is not the only field of interest in the study of light interaction with microorganisms. During the last 30 years, more interest has progressively been devoted to the development of closed photobioreactors (PBRs), aimed at the production of many substances of interest ranging from nutra- and pharmaceuticals, to bioenergetic compounds [4], [5]. As dense cultures are preferred to maximise production, light is normally the limiting factor to obtain a cost effective PBR operation. Although dense suspensions are a priori more appropriate for an efficient PBR utilisation [6], too concentrated cultures may increase operating costs [7] and completely deplete the system of light in most the external layers [8] as well. Therefore, optimisation of illumination conditions and cell density is required for improving overall photosynthesis performance and to minimise dark respiration and thus for achieving an optimal design of large-scale photobioreactors [9].

From the point of view of light propagation, there are important differences between the conditions in open waters or inside a PBR aqueous phase. The use of artificial light sources in many PBR set-ups, unnatural light cycles, the geometry of the arrangement itself and its inherent limitation in culture depth, not present in most open waters, are just some of the differentiating factors. A crucial topic is the question of stratification. Whilst in open waters a given equilibrium stratification is established within the photic zone and substantial differences may be found in microorganism concentration and composition depending on depth, inside a PBR efforts are usually oriented towards obtaining a good mixing so that the photosynthetic cells can rapidly move towards the external and internal zones of the reactor. Accordingly, the culture inside the PBR volume is usually regarded as being homogeneous.

Regarding the strategies to describe light distribution within water bodies, authors have either used algorithms that calculate the light field based on the radiative transfer equation describing light-matter interaction [10] or have applied stochastic methods such as Monte Carlo simulations [11, 12], which allow researchers to statistically follow the fate of individual photons within the medium. Relevant works based on this strategy have been published in the last decades. In this regard, in some cases the light field prediction is linked with experimental cell growth [13, 14] or coupled biomass production is modelled following a classical growth law such as Monod-type [15]. Several applications on different reactor shapes such as torus photobioreactors [16] or open ponds [17] can be found.

In our approach we aim at creating a procedure in between the simple light models and exceedingly detailed simulations in order to get a holistic view of the interaction of light and biomass based on the IOPs of the cells of interest, which has not been described in literature and is novel to the field. To do so, we will derive a relationship connecting the light field profile within a PBR suspension knowing the cell density, lamp emission spectrum, culture depth, absorption and scattering coefficients of the culture acclimatised to different light intensities. Making some simplifying assumptions we arrive at an expression that can be easily solved and can even give rise to an analytic relationship between operating parameters of the culture and includes in an implicit manner photo-adaptation of the cells. Furthermore, we have tested our scheme using information from two sources, completed with our own experiments, on two different strains of Synechocystis sp. PCC 6803 (hereafter referred to as Synechocystis), the wild-type and the Olive mutant. The latter is a strain with truncated phycobilisome structure, where the phycobilisome core is present but the rods are absent [18].

The model is able to predict the light attenuation caused by cultures in a considerable range of optical densities and light sources. Besides, the methodology proposed in this work follows a semi-mechanistic calculation procedure that can be generalised to other microorganisms and reactor geometries, whereas other published contributions are merely empiric fits or assume that absorption is the only factor for light attenuation. Moreover, this methodology is also capable of predicting spectral composition of light within the photic zone.

In the following subsections we will explain the main features of our modelling approach and its assumptions: section 2 exposes the experimental information and underlines how our method can be used in practice combining existing information with novel experiments. Section 3 discusses the results and highlights some interpretations that can be obtained from these analyses. Section 4 contains the conclusions and further outlook of our work.

1.1.2 Light spectrum influence in photosynthetic mechanisms

As stated before, light spectral composition in a PBR is sometimes not just a given condition, but can be selected and optimised. For an optimal selection of the light source, it is not only important to consider lamps whose emission peaks overlap the cell absorption spectra, but also other factors such as scattering, quantum yield and excitation balance between both types of photosystems [19].

Moreover, not only the light absorption capacity of the cells but also its efficiency in converting the captured photons into usable energy has to be taken into consideration. In this regard, the action spectrum represents the quantum yield of this efficiency upon light wavelength. It is important to note that the action spectra can vary depending on the pre-illumination conditions [20] or if supplementary light is applied. In the latter case, if cells are not exposed to some background light, the action spectrum can differ greatly from the absorptance spectrum in some wavelengths [21]. In other words, when using a monochromatic light source, the spectrum of the chosen lamp has to provide a balanced amount of quanta for both types of photosystems.

While it is common practice to study how white light affects growth in photosynthetic microorganism cultures, including mechanistic approaches for the photo-adaptation phenomenon [22], less research has been performed on how other types of light sources impact photosynthesis rates and related mechanisms. Specifically in cyanobacteria, some contributions can be found regarding light colour effect on oxygen evolution [23], redox state of the plastoquinone pool [24], growth [25] in Synechocystis, biomass composition of Arthrospira platensis [26] or areal biomass productivity in Chlamydomonas reinhardtii [27]. In Zavrel et al. research [25] and Markou contribution [26], blue light led to lower growth than red in both species, whereas in [27] yellow light promoted the highest productivity. Available irradiance as a function of the remaining wavelengths can shed light on real photosynthesis rates as quanta are absorbed by pigments which have specific absorption spectra on one side while part of the light is scattered in a spectrally dependent way. Particularly in Synechocystis cultures, blue is the most scattered colour and red the least [28], though this phenomenon relies on the type of organism and the aquatic environment [29].

Delving deeper in spectral composition of light publications, it must be noted that there are few experimental works which describe the wavelength dependent light distribution along the optical path-length. Measured spectra of remaining light within PAR range at different depths in cyanobacterial cultures of Spirulina platensis [8], suspensions of Chlamydomonas reinhardtii [16] and in Microcoleus chthonoplastes mats [30] are among the few. However, knowing the light field inside PBR cultures would help in designing large-scale flat-type PBRs and predicting growth conditions for maximal photosynthesis rates, e.g. optimal cell density and depth for given illumination conditions and species.

In summary, it is common to model and present photosynthesis as a function of the total white light intensity applied in the system as this approach is sufficient for validating general culture properties. However, knowing the spectral composition of light is necessary to deeply understand its effect on many photosynthetic processes.

1.2 Modelling framework definition

1.2.1 Inherent Optical Properties: definition and measurement

The two basic IOPs [31], the absorption and scattering coefficients, are defined on the basis of an imaginary, infinitesimally thin plane, parallel layer of medium, illuminated at right angles by a parallel beam of monochromatic light. AOPs, such as the different coefficients describing vertical attenuation, are properties of the radiation field depending not only on intrinsic features of the water body but also on the angular distribution of the light within the system as well as the depth.

Further, the photon complex and stochastic interaction in water due to both combined effects of absorption and scattering, does not lead to analytical solutions but in general can be treated only numerically. Photons can be either absorbed or scattered when interacting with matter, whereby in the first case they disappear and are transformed into a different type of energy such as heat or chemical bond excitations. In the case of scattering, the quanta direction and/or energy level is changed. Yet, thanks to inherent optical properties, absorption and scattering spectra of aquatic systems can be characterised.

In these terms, an incident monochromatic light beam, assuming energy conservation and no wavelength change due to scattering process, can be split into absorbed, scattered (both together considered as attenuated) and transmitted radiant flux [29]:

$$\Phi_a(\lambda) + \Phi_b(\lambda) + \Phi_t(\lambda) = \Phi_c(\lambda) + \Phi_t(\lambda) = \Phi_i(\lambda) \tag{1}$$

In practice it is not feasible to carry out measurements on infinitesimally thin layers, which implies the need to relate the absorption, scattering and attenuation coefficients, $a(\lambda)$, $b(\lambda)$ and $c(\lambda)$ respectively, with the measurable absorbance, scatterance and beam attenuance of finite thickness layers. To this purpose, spectrophotometer cuvettes can be used.

The beam attenuation coefficient $c(\lambda)$ can be linked with the attenuance measured by means of a spectrophotometer through the next equation [29]:

$$c(\lambda) = \frac{att(\lambda)}{r} \cdot 2.303 \tag{2}$$

where r is normally in the range of few centimetres in a typical spectrophotometer rectangular cuvette arrangement.

Absorption coefficient $a(\lambda)$ can be calculated in a similar way, although in this case the scattered light can distort the absorption measurement. Once it is reasonable to consider that all attenuation which arises from the scattering effect is small (e.g. by means of an integrative light collection sphere), the optical density or absorbance of the sample may be equated with the absorption coefficient analogously to the case of the attenuation coefficient shown in equation (2):

$$a(\lambda) = \frac{opd(\lambda)}{r} \cdot 2.303 \tag{3}$$

Now, from $a(\lambda)$ and $c(\lambda)$, it is straightforward to obtain the scattering coefficient $b(\lambda)$ as:

$$b(\lambda) = c(\lambda) - a(\lambda) \tag{4}$$

1.2.2 Estimation of main Apparent Optical Properties

The beam attenuation coefficient $c(\lambda)$ can give information about the attenuation properties of a water body depending on the wavelength, though it is not sufficient for estimating the real attenuation of light in the medium. To describe attenuation in a given propagation direction z, the downward irradiance attenuation coefficient $K_d(\lambda, z)$ is usually calculated, which is one of the most used AOPs and can appear in the well-known Beer-Lambert law [32]:

$$E_d(\lambda, z) = E_d(\lambda, 0) \cdot e^{-\overline{K}_d(\lambda) \cdot z} \tag{5}$$

As $K_d(\lambda, z)$ is an apparent property its determination is in principle only possible if the downward irradiance is measured in situ in the medium. Nevertheless, there have been some attempts to construct semi-empirical formulas that correlate this coefficient with inherent optical properties. By systematic calculation based on radiative transfer theory and Monte Carlo simulations, Phillips and Kirk in 1984 [33] found such a correlation, valid for a sun-illuminated water body and given by:

$$\overline{K}_d(\lambda, z) = \frac{1}{\cos\varphi_0}[a(\lambda)^2 + G \cdot a(\lambda)b(\lambda)]^{1/2} \tag{6}$$

where $G = 0.425\cos\varphi_0 - 0.190$, $\cos\varphi_0$ symbolises the cosine of the zenith angle of refracted photons just beneath the surface, while $a(\lambda)$ and $b(\lambda)$ are the absorption and scattering coefficients, respectively. As $K_d(\lambda, z)$ does not significantly depend on the depth within the euphotic range, it can accepted that this parameter remains constant within this region and rewrite it as $K_d(\lambda)$. An application example for modelling oceanic water light attenuation using equation (6) can be found in [3].

In our contribution we will assume that the same physical principles that led to the above relationship apply to the particular case of light propagation within a PBR. In the case of a flat-type PBR placed in a laboratory, illumination is usually perpendicular to the panel planes and hence, the cosine of the zenith angle $\cos\varphi_0$ in equation (6) is one. G represents the contribution of scattering with respect to absorption and under these perpendicular illumination conditions equals 0.235. In the case of a flat type PBR placed outside and illuminated by the sun, the position of the sun should be taken into account through the zenith angle.

The combination of equations (5) and (6) may in principle be used to estimate light field attenuation for a given wavelength based on previously measured inherent optical properties of the organism of study. Nevertheless, radiometric measurements used to evaluate the light field in a water body are often not specifically sensitive to wavelength and as a result simply collect those photons within the so-called Photosynthetic Active Radiation (PAR) (about 400 to 700 nm), treating them as a single value. In such situation it is more appropriate to use AOPs that represent the whole PAR [29], by accepting the hypothesis that the validity of the Beer-Lambert relation, displayed in the expression (5), can be extended to the whole PAR range:

$$E_{d,\text{PAR}}(z) = E_{d,\text{PAR}}(0) \cdot e^{-\overline{K}_{d,\text{PAR}} \cdot z} \tag{7}$$

Besides, PAR irradiance is given as:

$$E_{d,\text{PAR}}(z) = \int_{400}^{700} E_d(\lambda, 0) \cdot e^{-\overline{K}_d(\lambda) \cdot z} d\lambda \tag{8}$$

Combining equations (7) and (8) and rearranging terms we find the following expression for $\overline{K}_{d,\text{PAR}}$:

$$\overline{K}_{d,\text{PAR}} = -\frac{1}{z}\ln(\int_{400}^{700} \rho E_d(\lambda, 0) \cdot e^{-\overline{K}_d(\lambda) \cdot z} d\lambda) \tag{9}$$

where $\rho E_d(\lambda, 0)$ represents the spectral photon flux density that measures the relative contribution of the different wavelengths to $E_d(\lambda, 0)$, commonly referred to as the lamp emission spectrum. Although the depth variable z appears in the former relation, the $\overline{K}_{d,\mathrm{PAR}}$ value remains basically constant up to depths in which the spectral composition of light has substantially changed in comparison with that of incident light. This change in spectral composition is due to the fact that photons corresponding to green wavelengths are less frequently absorbed. At larger depths, thus, the $\overline{K}_{d,\mathrm{PAR}}$ value will converge towards the smaller attenuation coefficient of monochromatic green light.

1.2.3 Calculation of the average light intensity

When dealing with microorganisms the analysis of their optical properties is much more complicated, as many other factors must be taken into consideration: the growth medium, the fitness of the culture and even the fact that cells must be able to acclimate to varying light intensities and changes in light spectrum. This latter property specially makes the question much more difficult for a mathematical treatment, as IOPs keep memory of the light conditions which cells have been previously subjected in such a way that in essence: $a = a(\lambda, E_d(t', \lambda'))$ and $b = b(\lambda, E_d(t', \lambda'))$ $\forall t' \in [t - t_{acc}, t], \lambda' \in$ PAR. This expression reflects the fact that the IOPs (and thus all related AOPs) depend on the intensity, spectral distribution and time evolution of light during the immediately previous acclimation time window, which ranges from hours to days [34] and is represented by t_{acc}.

Within a PBR running under stationary conditions the question can be substantially simplified considering the average light intensity as an indicator of bioengineering properties. Such approach has been repeatedly used since 1962 when it was applied for estimating growth in dense cultures [35]. When cells are moving along the whole optical path-length and are homogeneously distributed, it is reasonable to accept that all are exposed in time-average to the same intensity and light spectrum which equals the mean value of light irradiance within the PBR volume. Given that optical conditions are constant during a sufficient lapse of time (at least longer than t_{acc}), cells will physiologically adapt to this, a priori unknown, average light intensity [36]. Our model will develop this idea, though it should be noted that for cells growing in fluctuating light conditions, photosynthetic performance will additionally depend on the dynamics of the fluctuating light regime, that is, not only on the overall time exposure to light and darkness but also on the switch frequency [37].

To correlate the experimental conditions in which the IOPs a and b are measured or characterized with a given PBR experiment we express them as follows:

$$j(\lambda, E_{d,acc}) = \rho_{Chla} \cdot j^{\star}(\lambda, E_{d,acc}) \qquad j = a, b \tag{10}$$

where $E_{d,acc}$ is a constant acclimation downward PAR light intensity to which cells were exposed during a time interval $t \geq t_{acc}$ before measurement took place, $a^{\star}(\lambda, E_{d,acc})$ and $b^{\star}(\lambda, E_{d,acc})$ are chlorophyll a-specific absorption and scattering coefficients corresponding to cells which have been acclimated to these intensities. Equation (10) also assumes that the IOPs are in a linear relationship with the amount of chlorophyll a (hereafter referred to as chl a) present in the PBR suspension. Similarly, for attenuation coefficients it is possible to define total and chl a-specific magnitudes. Given that we have characterized our cells in a sufficiently representative range of acclimation intensities $\{E_{d,acc_1}, E_{d,acc_2} \cdots E_{d,acc_n}\}$ we can, through interpolation, construct functions $a(\lambda, E_{d,acc})$ and $b(\lambda, E_{d,acc})$ that allow us to calculate the IOPs for any given intensity within that range. Then, using (6) it is possible to obtain the corresponding function that represents the downward attenuation coefficient:

$$\begin{aligned}\overline{K}_d(\lambda, E_{d,acc}) &= \rho_{Chla} \cdot \overline{K}_d^{\star}(\lambda, E_{d,acc}) = \\ &\rho_{Chla} \sqrt{a^{\star}(\lambda, E_{d,acc})^2 + G \cdot a^{\star}(\lambda, E_{d,acc})\, b^{\star}(\lambda, E_{d,acc})}\end{aligned} \tag{11}$$

for any given value of the volume-average irradiance intensity. Rewriting equation (6) and taking into account expression (10):

$$\overline{K}_{d,PAR}(E_{d,acc}) = -\frac{1}{z} \ln\left(\int_{400}^{700} \rho E_d(\lambda, 0) \cdot e^{-\rho_{Chla} \cdot \overline{K}_d^{\star}(\lambda, E_{d,acc}) \cdot z} d\lambda\right) \tag{12}$$

In a usual PBR experiment in which cells do have time to acclimate to the long-term conditions, the average light intensity in the reactor must be found as the solution of a non-linear equation. To illustrate the idea, in the particular case of a flat plate reactor with one-sided illumination from one single planar light source we can for instance calculate the average light intensity as:

$$\begin{aligned} E_{d,acc} &= \frac{E_{d,\text{PAR}}(0)}{L} \int_0^L e^{-\overline{K}_{d,\text{PAR}}(E_{d,acc}) \cdot z}\, dz \\ &= E_{d,\text{PAR}}(0)\, \frac{1 - e^{-L \cdot \overline{K}_{d,\text{PAR}}(E_{d,acc})}}{L \cdot \overline{K}_{d,\text{PAR}}(E_{d,acc})} \end{aligned} \tag{13}$$

which can be solved numerically for the unknown value $E_{d,acc}$ of the average light intensity equal to the acclimation intensity in the PBR, whose depth is L.

Expression (13) can be understood as a self-consistency condition between the average intensity of the light field inside the PBR and the resulting attenuation coefficient, but we would like to stress that this particular form is valid for the case of a one-side illuminated flat panel (or for a two-side illumination set-up where incident intensity would be half for maintaining equivalent conditions). For other geometric configurations (e.g. multiple panel arrangements, tubular PBRs) the concept remains the same, but $E_{d,acc}$ will have a different formal expression. In any case, our methodology is easily extensible to these other cases. In the following, we will refer to this approach as Auto-consistent Field Approximation algorithm (AFA).

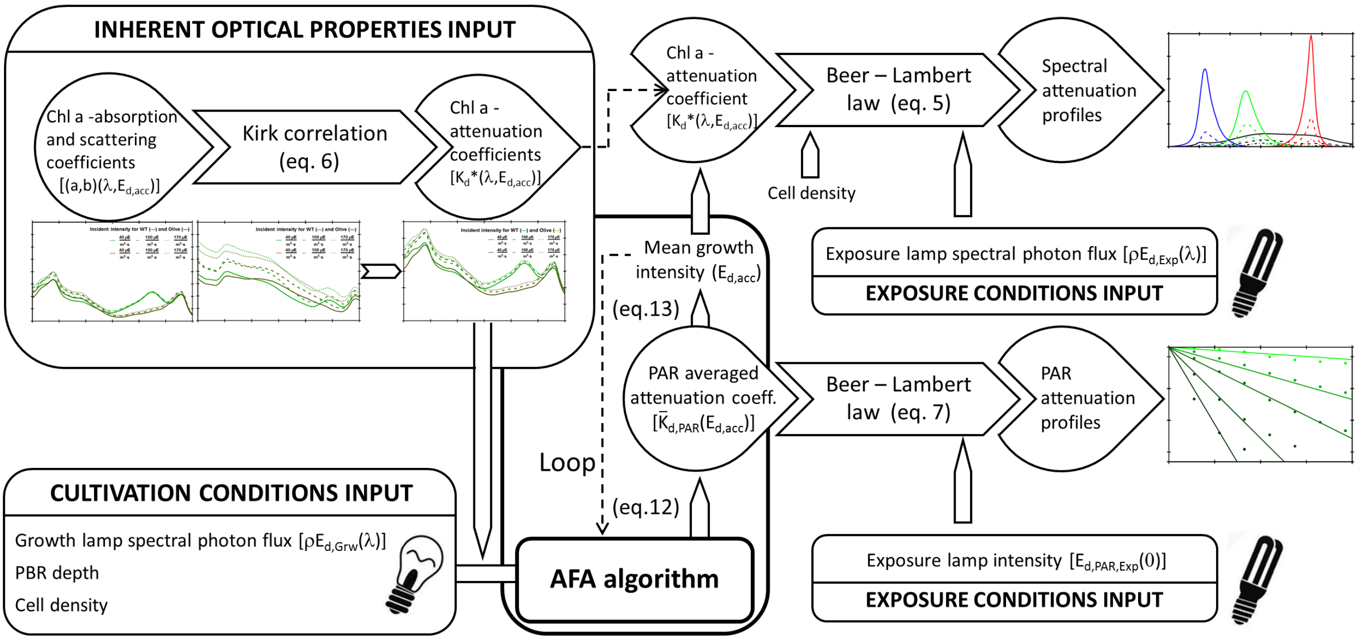

Figure 1: Summarised modelling scheme to obtain PAR attenuation profiles and spectral ones.

2 Materials and Methods

2.1 Validation strategy and modelling scheme implementation

To test the predictability of our method, we measured the IOPs of two similar organisms, wild-type (WT) and Olive strains of Synechocystis in tightly controlled PBR conditions [34] to calculate their specific attenuation coefficients, $\overline{K}^{\star}_{d}(\lambda, E_{d,acc})$. We then used these coefficients to deduce the actual attenuation of light in cultures of the same organisms characterized by Lea-Smith and his co-workers in different experiments [38], and compare them with the actual measured attenuation coefficients. The in silico work was integrally performed in $Mathematica$ 10.4.

2.1.1 Measurement of the IOPs spectra and calculation of the attenuation coefficient function

Before taking the optical properties measurements, Synechocystis cultures were grown in stable conditions so that they got acclimatised to mean irradiance. Cells were grown in a 5 litres flat-bed photobioreactor with a surface-to-volume-ratio of 50 m^{-1} and a depth of 4 cm at constant pH of 7.0 and temperature value of 30 °C in continuous operation after they were inoculated [34]. Cell density was maintained constant under turbidostatic process control. Cells were cultivated for at least 48 hours till a constant growth rate was established.

We analysed Synechocystis cultures, namely wild-type strains and the truncated antenna Olive mutants to obtain their specific absorption and scattering coefficients in stable PBR conditions to ensure that organisms are acclimated to the same intensity in enough time. To this purpose, absorbance and attenuation spectra within the PAR range were measured at every nanometre after cultivating cells at three different incident light intensities, $40, 100$ and 170 $\mu mol\, photons \cdot m^{-2} \cdot s^{-1}$ of cool white LED lamp, covering the usual range of intensities that cells may encounter inside a PBR. After stabilization of the culture at an OD_{750} value of 0.5, a sample was taken to measure absorptance and attenuance of the cells in the different conditions.

Optical measurements of the samples were performed by means of a Shimadzu UV2450 UV-vis spectrophotometer equipped with an integrating sphere for absorbance measurements. The latter device is a double-beam system integrating sphere (ISR-2200) whose internal diameter is 60 mm with $BaSO_4$ inside coating. The culture samples were previously diluted to reduce effects of self-shading and multiple scattering, keeping the maximum optical thickness at 400 nm, well below 0.3, a threshold consistent with a given criterion [39]. This guarantees that the measured optical coefficients are inherent rather than hybrid optical properties [1]. Finally, the total scattering coefficient, b, for all angles (except for the acceptance angle of the photomultiplier tube 0 to 5 degrees) was determined by subtracting the beam attenuation, c, from the true absorption coefficient, a.

From these measurements and by means of equations (2), (3) and (4) a set of 3 spectral absorption and scattering coefficient-functions, $a(\lambda, E_{d,i})$ and $b(\lambda, E_{d,i})$, where $i = 40, 100, 170$, and their corresponding chl a-specific functions $a^{\star}(\lambda, E_{d,i})$ and $b^{\star}(\lambda, E_{d,i})$, where $i = 40, 100, 170$ were derived. The results are shown in Fig. 4.

However, it is important to note that the real acclimation intensities of the cultures are lower than the referred to above incident intensity values of either $40, 100$ or 170 $\mu mol\, photons \cdot m^{-2} \cdot s^{-1}$. To find the correct acclimation intensities an iterative procedure was followed using our proposed AFA-algorithm. A summarised scheme of the whole calculation process is shown in Fig. 1. There it can be seen that the methodology transforms the required input, i.e. lamp characteristics during growth phase, cell-density, optical path-length and attenuation function, into the mean acclimatisation intensity and PAR averaged attenuation coefficient. This is done in a close loop between these two magnitudes. Afterwards, both can be used to obtain light field distribution using Beer-Lambert law. If it is desired to apply the attenuation coefficient function with spectral resolution $\overline{K}_d(\lambda, E_{d,acc})$, different attenuation results will be obtained for each wavelength and intensity, whereas in the case of the PAR related coefficient $\overline{K}_{d,PAR}(E_{d,acc})$, the attenuation is just a single representative value and the coefficient is directly estimated by means of the algorithm solution. Though in any case, the Beer-Lambert equation remains the same and just the coefficient has a different meaning. Moreover, the method allows one to estimate culture attenuation with cells owning previous optical properties but exposed to different illumination conditions. However, we will normally be interested in assessing the light field in a PBR system where cells are growing, so exposure and cultivation conditions (including lamps) will be the same.

This procedure can also be applied to estimate the mean irradiance in our PBR set-up at different lamp intensities by updating the total attenuation and mean irradiance and checking its convergence:

1. First $\overline{K}_{d,\text{PAR:0}}$ is calculated assuming that the acclimation intensities in the different experiments were the nominal set "0"= $\{40, 100, 170\}$,$\mu mol\, photons \cdot m^{-2} \cdot s^{-1}$. To do so, we just need to substitute these values in equation (12), which integrates the reconstructed attenuation spectra (Figure 6) at the given intensities to deliver the $\overline{K}_{d,\text{PAR:0}}$ PAR attenuation coefficients.

2. Thanks to these parameters, we can estimate in a straightforward manner the corresponding set of acclimation intensities in the PBR by directly substituting $\overline{K}_{d,\text{PAR:0}}$ in equation (13). In this manner, a new set of acclimation intensities "1" $\{E_{d,acc,40:1}, E_{d,acc,100:1}, E_{d,acc,170:1}\}$ is obtained.

3. With this new set of irradiance values, the new $\overline{K}_{d,\text{PAR:1}}$ is calculated and, again solving same equations for each of the three experiments, a further set of acclimation intensities "2" $\{E_{d,acc,40:2}, E_{d,acc,100:2}, E_{d,acc,170:2}\}$ is obtained.

4. One can see that in just a couple of iterations the acclimation intensities converge to a stable value, which will be considered the final acclimation intensities that are used to reconstruct the organism specific attenuation coefficient function: $\overline{K}^{\star}_{d}(\lambda, E_{d,acc})$.

5. The obtained final average irradiance, given as a percentage value, with respect to our three studied lamp intensities are 48%, 49% and 60% for WT and 59%, 60% and 61% for Olive. The higher value for the case of WT cultures grown at 170 $\mu mol\, photons \cdot m^{-2} \cdot s^{-1}$ is due to a considerable reduction in the chlorophyll concentration and this causes the total attenuation to drop. The estimated irradiance fits well with previous estimation of other authors for the WT strain [40].

It is remarkable that for calculating the light field in any further condition, the same approach is used: from incident irradiance values, PAR coefficients first and related average irradiance values are obtained in a self-consistent way in a few iterative steps.

2.1.2 Application of the derived attenuation function to experiments

In a completely independent way, Lea-Smith and his co-authors measured the light field of WT and Olive Synechocystis cultures grown in the same optical environment but momentarily exposed to a variety of conditions (to in situ measure the light distribution), including different types of light sources.

With our proposed approach it is now possible to use the reconstructed function $\overline{K}_d^{\star}(\lambda, E_{d,acc})$ together with the rest of the required input information to first estimate $\overline{K}_{d,\mathrm{PAR}}(E_{d,acc})$ and thanks to it, the attenuation profiles.

To benchmark our in silico predictions with the experiments described in the referenced work, several specific parameters, namely the values of ρ_{Chla} and $E_{d,acc}$ must be additionally deduced, which requires some knowledge and analysis of how the measurements were performed. Moreover, as light field samples were linked to OD_{750} values, the referenced chl a concentration for WT and Olive cultures per OD_{750} unit in that contribution is used, which is 5400 and 5300 mg chl a for WT and Olive, respectively.

2.1.3 Description of the experimental set-up and deduction of the relevant parameters from the published measurement results

As described in the referenced work [38], cell suspensions of around 5 cm were first grown in conical flasks under 120 $\mu mol\, photons \cdot m^{-2} \cdot s^{-1}$ halogen white light. By means of an elemental geometric analysis which is dependent on the shape of the flask, we have deduced an equivalent optical path-length of $4\ cm$. Anyhow, these types of approximations, due to our lack of exact knowledge about how the experiments were made, are necessarily prone to a certain degree of uncertainty.

After reaching the desired OD_{750} values and in order to perform the attenuation trials, the cells were transferred to an 11 cm custom made apparatus used for measuring light penetration at different depths (in which several light detectors where located every 11 mm up to 110 mm). For our analysis we will depart from the consideration that since the attenuation experiments were done shortly after the cells were transferred to the new vessel, the acclimation intensity of the cells, and thus their spectral $K_d^{\star}$ function corresponds to the acclimation intensity within the conical flask in which they have been grown.

The Synechocystis attenuation data set is composed of light intensity values at increasing depths for the strains here studied plus two extra antenna mutants (not assessed in this contribution), all of them exposed to white LED light at 5 different OD_{750} values (0.1, 0.5, 1.0, 2.5, 5.0) and at three different irradiance values (500, 1,000 and 2,000 $\mu mol\, photons \cdot m^{-2} \cdot s^{-1}$), summing a total of 15 white light experiments. Additional blue, green and red LED light trials were carried out at an OD_{750} value of just 1.0 and 1,000 $\mu mol\, photons \cdot m^{-2} \cdot s^{-1}$ of light intensity. The emission spectra of the four LED lamps used in the different experiments are represented in Fig. 2.

It is worth stressing the assumption that cells didn't have enough time to adapt to the new environment and consequently they simply expressed their optical properties arising from the previous growth environment in the flasks and not from the attenuation experiment conditions in the custom made attenuation measurement device. Indeed,

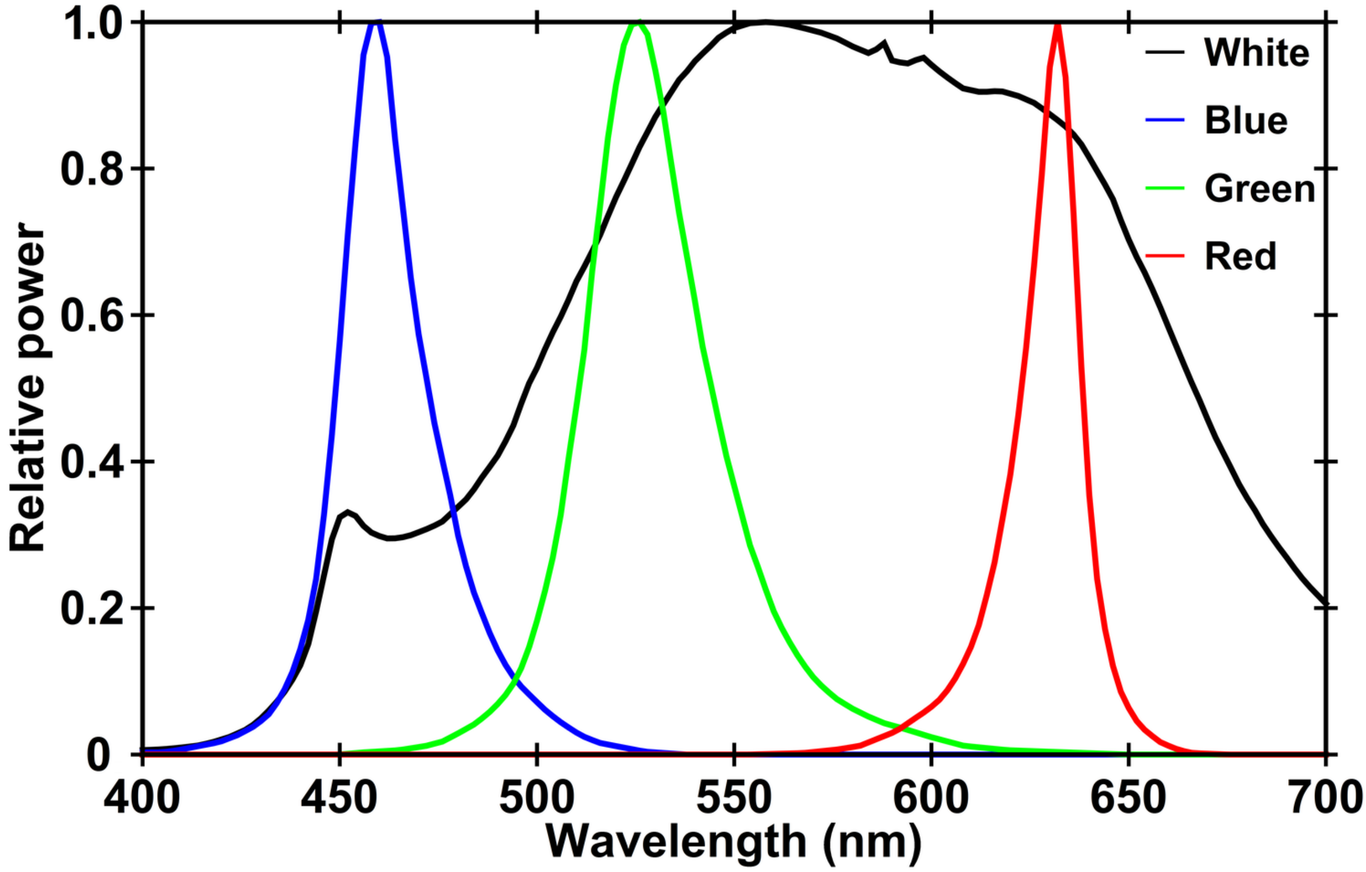

Figure 2: Emission spectra in terms of relative power of the LED lamps used for the attenuation trials. Graph colours represent each LED characteristic colour (blue, green and red), whereas black curve corresponds to the white LED.

though cultures were exposed to 500, $1,000$ and $2,000$ $\mu mol\, photons \cdot m^{-2} \cdot s^{-1}$, they presented a similar attenuation coefficient in the original work for any given cell density, supporting our hypothesis.

Other differences in the growth conditions among both laboratory set-ups should be discussed, specifically those connected with the differences in the spectral characteristics of the light sources used. The cells grown in [38] were cultivated with halogen lamps whereas for estimating Synechocystis IOPs, we employed a cool white LED light. This may in principle generate differentiated optical properties in the cells, but both lamps spectra have quite a wide band of action in the PAR range, a similar shape, and they can mainly be distinguished by the blue peak of the cool white LED spectrum. As Synechocystis cells have the capability to reorganise the photosynthesis apparatus for balancing light input in order to seek optimal growth, we would expect a similar light absorption and scattering profile of the cells cultured under the light of these two lamps. A distinct outcome would be expected if a light source with non-equivalent emission spectrum profile would be employed. In fact, in marine Synechocystis cultures (Synechocystis sp. BCC010, Banyuls collection) grown under blue or green light, the measured spectra had a slightly different shape and half of the amplitude of those corresponding to cells cultivated under similar conditions with white light [28].

We thus conclude that the attenuation coefficients measured in the attenuation assays by Lea-Smith and co-workers should correspond to the acclimation intensity within which the cells were grown in the conical flasks. To find these intensities from the original experiments, we solved, for each of the conditions, the non-linear equation that allows us to obtain such intensity self-consistently. The corresponding expression for the acclimatisation irradiance is given in equation (13), with $E_d(0) = 120\, \mu mol\, photons \cdot m^{-2} \cdot s^{-1}$, $L = 4\, cm$ and ρ_{Chla} deduced from the corresponding OD_{750} value in each experiment.

2.2 Linearity check of the K_d vs. OD_{750} relationship

In our light field model, we ultimately relate a given value of an OD_{750} to which cells have grown to a given chl a concentration and subsequently to a downward attenuation coefficient. In this regard, it is important to assess the limits of the validity of such an assumption. What respects the OD_{750} vs. chl a relationship, in Fig. 3 it is shown that in our experiments the relationship between chl a and OD_{750} remains approximately linear for the studied OD range in both WT and Olive strains grown at a nominal PBR intensity of $100\, \mu mol\, photons \cdot m^{-2} \cdot s^{-1}$.

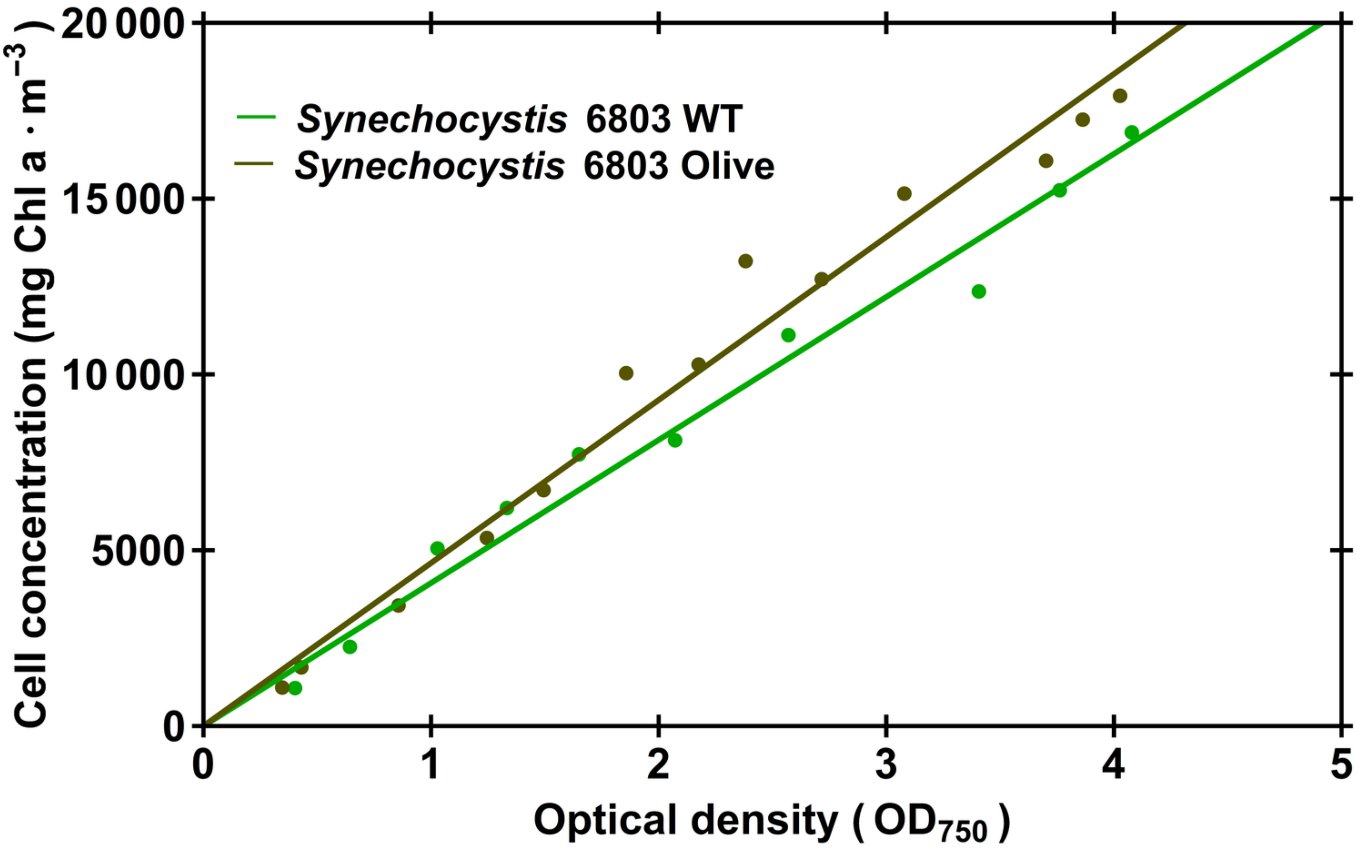

Figure 3: Relationship between chlorophyll a and OD_{750} value of both strains (WT in green colour and Olive in brown one) grown at incident $100\, \mu mol\, photons \cdot m^{-2} \cdot s^{-1}$. Dots represents experimental data and the line represents the lineal regression.

There are, apart from these analysed experiments, further empirical data that support our hypothesis of a linear behaviour between attenuation coefficient and cell density in dense cultures. In this context we may mention the contributions of Zhang and co-workers, that in Synechocystis cultures studied the ratio of cell concentration as dry weight to the PAR attenuation coefficient [40]. Gitelson and co-workers worked with Spirulina platensis cultures, where the relationship between chl a concentration and spectral attenuation coefficient were found to be almost constant for a wide range of cell concentrations [8]. In both mentioned contributions, we can find the maximum reported cell concentration equivalent up to 4 OD_{750} units, practically covering the same range of densities as in our research.

Moreover, there is one publication where poly- and monochromatic light attenuation in dense and ultra-dense cultures of the green alga Chlorella vulgaris were analysed [41]. It was reported that attenuation coefficients augment linearly with the cell concentration up to values of around 300 m^{-1}, which is in agreement with our modelling hypothesis. Above this value the relationship tends to get saturated.

3 Results and discussion

3.1 Optical spectra and analysis of the resulting IOPs

As a first outcome, the chl a absorption for both strains resemble each other significantly in shape and amplitude as it is shown in Fig. 4 (A). Olive spectra lack the absorption of phycocyanin pigment in the orange range and have a slightly larger absorbance in the blue band due to a somewhat higher carotenoid presence, as was already reported [42]. Phycobilisomes appear not to be dismantled at moderate light intensities within our irradiance range, as the absorption peak of phycocyanin doesn't progressively drop as it does in the case of the marine Synechocystis WT strain [28]. The fact that chl a-specific absorption spectra show a constant absorption peak at 675 nm is expected, since absorption in this band is mainly caused by chl a itself in Synechocystis and to a much lesser extent due to allophycocyanin pigment [43]. Indeed, all spectra have a local maximum value of around 0.22 $m^2 \cdot mg\ Chla^{-1}$ at 675 nm for Olive and a similar one of 0.20 $m^2 \cdot mg\ Chla^{-1}$ for the WT Synechocystis. In [28] similar values were reported for this wavelength.

Scattering spectra, shown in Fig. 4 (B), are likewise practically identical in both studied strains and have local minima close to the absorption peaks. The shift of the peaks to slightly shorter wavelengths with respect to the absorption ones can be explained by the anomalous dispersion theory [44]. Furthermore, the likeness in their shape is an anticipated outcome as both strains have comparable cell diameters [38], similar chl a amount and pigment composition [42]. It is noteworthy that the ratio between scattering and absorption coefficients at a given intensity in both strains is much lower than in the Synechocystis marine strain, because in the latter, chlorophyll a content per cell was 5 to 8 times lower and thus its absorption capacity was also lower.

Absorption and scattering in m^{-1} units show a different behaviour with respect to their chlorophyll referenced magnitudes: scattering remains constant for all intensities, whereas absorption coefficients slightly decline with increasing intensities, especially at 170 $\mu mol\, photons \cdot m^{-2} \cdot s^{-1}$.

To quantitatively assess the relative importance of scattering in both studied strains, from equation (6) it can be easily deduced that the term $G \cdot b(\lambda)/(a(\lambda) + G \cdot b(\lambda))$ quantifies the influence of scattering in total attenuation as its complement to one, $a(\lambda)/(a(\lambda) + G \cdot b(\lambda))$, would approach unity in an hypothetical, infeasible "absorption without scattering" scenario. According to this analysis, within PAR 60% to 90% of attenuation is due to absorption for both strains, see (Fig. 5). As expected, there is an exception in the green band where absorption is much lower due to the Synechocystis lack of specific absorption pigments for this band. In addition, higher light intensities lead in both strains to an increased scattering contribution (though scattering coefficient itself keeps constant) at the expense of a lower absorption participation because at higher irradiance values, cells pigment concentration is in generally decreased with the exception of carotenoids, so cells do have less chances to capture photons, meanwhile they have a higher probability to be scattered along the optical path-length. It has to be noted that scattering itself doesn't contribute to the disappearance of photons as they can only be taken out of the medium by the biomass or the water body absorption but it can effectively contribute to an increased light attenuation due to longer optical path-lengths.

Furthermore, averaging along the PAR range and taking into consideration the emission spectrum of the different LED sources, the overall influence of photon scattering/absorption as a percentage value can be estimated. For white LED source illumination, approximately one third of attenuation depends on scattering in the WT strain, while in Olive this value is slightly higher. In the propagation of green light, scattering shows a stronger influence (50%), while the opposite occurs in red light attenuation (20%). As light intensities increase, scattering tends to play a more significant role, especially for the WT strain, though this increase is not remarkable in the range of studied irradiance (data not shown).

3.2 Attenuation profiles for white light exposure

In order to estimate attenuation within the cultures, chlorophyll-specific spectral coefficient functions $\overline{K}_d^{\star}(\lambda, E_{d,acc})$ have to be calculated first. This function at the three acclimation intensities display a similar shape as the absorption spectra, but with higher values at the blue band due to the increased contribution of scattering in this range (Fig. 6). Maximum values at 440 nm are comprised between 0.045 and 0.055 $m^2 \cdot mg\, Chla^{-1}$ in both strains. It might seem that as the chlorophyll-specific attenuation coefficients increase somewhat upon irradiance, total attenuation should follow this trend. But it has to be noted that as light intensity increases, chlorophyll concentration in the cell drops and so does the total attenuation. By multiplying the chlorophyll-specific attenuation coefficients by the chlorophyll amount at each light intensity, the total downward attenuation coefficient can be calculated. In this regard, total attenuation coefficients in m^{-1} get gradually reduced with increasing intensities (data not shown) due to smaller absorption coefficients. Besides, the attenuation spectra have values between $70 - 90\ m^{-1}$ in both strains at $440\ nm$, which are quite close to the ones reported for Spirulina platensis [8], a cyanobacterium with comparable pigment composition and absorption spectra shape, given similar cell chlorophyll concentrations.

Following the corresponding calculation pipeline summarised in Fig. 1, attenuation profiles (intensity vs. depth within the measurement assay) are obtained. They correspond to attenuation for cells grown under white halogen light and momentarily exposed to different white LED light intensities at several OD_{750} values. The experimental irradiance-weighted attenuation coefficient of five different cell-density concentration samples (0.1, 0.5, 1.0, 2.5 and 5.0 OD_{750}) at 2,000 $\mu mol\, photons \cdot m^{-2} \cdot s^{-1}$ incident irradiance are hereby compared with the attenuation coefficient (or more rigorously, with the mean downward attenuation coefficient averaged within PAR range $\overline{K}_{d,\mathrm{PAR}}$) resulting from our simulation method. In Fig. 7 (A) and (B) for WT and Olive strain respectively, it can be seen that there is a reasonable correlation between experimental and in silico results. Small discrepancies arise for the case of the most diluted cultures, where the attenuation is somewhat underestimated in both strains, though data do not show a clear tendency. Relative error for the attenuation coefficient comparison at this cell concentration is quantified to be around 25% in WT strain, 30% in Olive and much lower in the other density cases for both strains. At this OD (0.1 OD_{750}), we estimated the acclimation irradiance to be around 90% of the nominal incident value of 120 $\mu mol\, photons \cdot m^{-2} \cdot s^{-1}$. At this average intensity, expressed as a percentage of the incident irradiance at depth $z = 0$, the total attenuation coefficients (in m^{-1}) suffer little bit higher variations and particularly started to decline in our laboratory WT strain (data not shown). On the contrary, at higher cell-densities the average irradiance is lower, around 20 $\mu mol\, photons \cdot m^{-2} \cdot s^{-1}$, and in this light environment optical spectra do not vary much at different light intensities and thus the uncertainty of the irradiance level has a minor impact on the light decay slope.

Particularly in the case of Olive cultures it is noteworthy to mention that, as in the case of the WT suspension profiles, the model predicts the attenuation for all OD_{750} values quite accurately with the exception of the Olive samples at the OD_{750} value of 2.5 then the corresponding attenuation is overestimated (associated error of 14%).

The estimated average irradiance inside the simulated cultures of 0.5 OD_{750} in Lea-Smith et al. experiment conditions, is 45% and 56% for WT and Olive strain, respectively. These are very close to the ones that were hypothesised (49% and 60%) to assess the average irradiance in our laboratory conditions (same reactor depth, density and very similar lamp irradiance, 100 instead of 120 $\mu mol\, photons \cdot m^{-2} \cdot s^{-1}$), reinforcing the auto-consistency of our algorithmic approach with respect to attenuation.

Finally, in order to better appreciate the general trend for all the densities, experimental and theoretical chl a-specific downward attenuation coefficients $\overline{K}^{\star}_{d,PAR}$ were obtained and plotted together. To do so, the experimental data set that was described above and is shown in Fig. 7 (A) and (B) for each strain was used to estimate the experimental downward attenuation coefficients. More precisely, the irradiance-weighted attenuation coefficients were calculated and compared with our results. As displayed in Fig. 8, the model is able to predict the tendency of the coefficients. It is noteworthy to remark that as the cell-density increases, the average irradiance (and the attenuation coefficient) gradually decreases. Accordingly, if ultra-dense cultures were employed, the mean light intensity would tend to zero. In this hypothetical situation, cells would not have enough energy to sustain biochemical processes and probably long-term adverse effects would appear in metabolism that could impact the optical properties.

3.3 Attenuation profiles for colour light exposure

Next, we benchmark our modelled attenuation results with the experiments carried out again by Lea-Smith and co-workers, in which cultures were exposed to blue, green, red and also white LED light at a single optical density of 1.0 OD_{750}. In this case the irradiance used to measure attenuation was $1,000\ \mu mol\, photons \cdot m^{-2} \cdot s^{-1}$, instead of $2,000\ \mu mol\, photons \cdot m^{-2} \cdot s^{-1}$.

Regarding this data assessment, we were not initially able to properly model the sample points: obtained simulated profiles following the previously described reasoning were only matching experimental data for white light in both strains, and red in the WT strain. In the other cases, the model clearly underestimated the experimental sample values. This modelling mismatch occurred for both strains, and hence, the simulation using one colour series of data was adjusted to check if knowing the average irradiance would be sufficient to correctly predict the light decay in all cases.

This procedure was used with the WT culture blue light assay (Fig. 7(C)) by calculating the acclimation irradiance in the growth conditions that would allow one to fit the data. It was found that the acclimation light intensity that delivers satisfactory results is 40% higher than the value that was supposed to exist inside the conical flasks for both strains. Interestingly, only changing this value, the remaining five experiments analysed in this subsection and plotted in Fig. 7(C) and Fig. 7(D), for WT and Olive mutant respectively, were correctly predicted. One reason to explain this unexpected growth irradiance could be that cultures had been kept in other illumination conditions for some period of time, consequently having adapted and changed their absorption capacity before the attenuation measurement. Moreover, green colour is in many cyanobacterial cultures the one that is less attenuated and this is also the particular case in Synechocystis suspensions. This fact also supports our idea that, for this series of experiments, there are two groups of cultures, each one acclimatised to a different mean irradiance. Indeed, Fig. 7(C) displays the attenuation for WT cells illuminated with the four different LED lamps and unexpectedly green attenuation seems to be higher than white one though all cells have been cultivated in the same conditions and thus green should be the least attenuated colour.

Hence, we have adopted the working hypothesis that the assays described in this section correspond to cultures acclimatised to two different light conditions, thus possessing two differentiated "optical footprints" and by assuming this fact, we have been able to precisely estimate light attenuation at different exposure LED light in both strains. Analysing the results in more depth by comparing both strain profiles for a given light colour, it is obvious to realise that blue and green attenuation are quite similar in both strains, around 165 m^{-1} for blue light, 81 and 95 m^{-1} for green radiation in Olive and WT strain, respectively, whereas red attenuation in Olive has clearly diminished due to the lack of phycobilisome antennas. For this colour downward attenuation coefficient accounts for 125 m^{-1} in WT.

In contrast to white light exposure assays, these trials show a purely exponential decay. On the other side, when observing white light attenuation, a two-zone behaviour around a turning point of approximately 1% (20 $\mu mol\, photons \cdot m^{-2} \cdot s^{-1}$) of incident irradiance is apparent. Below this threshold attenuation diminishes. As already mentioned, white light is comprised by different wavelengths and in general green light is the least attenuated. When most light has been absorbed by the medium, only green radiation remains in the PBR and thus a smaller attenuation is expected. This can be better understood from our simulations shown in Fig. 10 where the initial white light lamp emission spectrum is gradually transformed into a green colour one.

3.4 Spectrally dependent penetration depth and attenuation

The previously described results correspond to the integrated attenuation within the PAR range. This type of measurement is a more common and practical way to evaluate irradiance and therefore it is much easier to find information of trials on PAR attenuation in photosynthetic microorganisms rather than to describe the spectrally-dependent light attenuation within the cultures. Further, to calculate the light penetration with spectral resolution, we have to solve Beer-Lambert equation for the distance inside the culture at which the irradiance falls to a threshold value, for instance the 10% of the initial photon flux for each wavelength. This value roughly represents the limit depth at which net cell respiration will occur at the simulated conditions of this subsection.

To check that our algorithm also delivers reliable results when purely spectral assessment of light is taken into consideration, an extensive literature review was conducted in order to find relevant contributions with such type of measurements. Unfortunately, we did not find any analogous experiments on Synechocystis and therefore we looked into available attenuation coefficients and penetration profiles with spectral resolution of cyanobacterial species such as Spirulina platensis M-2, a species which is very close to Synechocystis. Suspensions of this organism at very high concentrations were examined and penetration depths measured [8]. These wavelength-dependent depths were not directly estimated but calculated from experimentally obtained values of $K_d(\lambda, z)$, measuring the downward light flux with a radiometer at the surface and at some depth within the cell suspension.

So, we simulated Synechocystis WT cultures at typical PBR densities, i.e. 1.0 OD_{750}, and acclimatised to a lamp irradiance of 80 $\mu mol\, photons \cdot m^{-2} \cdot s^{-1}$, which approximately corresponds to an incident irradiance of almost 200 $\mu mol\, photons \cdot m^{-2} \cdot s^{-1}$ in a 4-cm deep PBR. Then we benchmarked our strain penetration profile with the Spirulina one that would arise from cells of the latter organism owning similar spectral attenuation coefficients $\overline{K_d}(\lambda, [z_1, z_2])$. If we assume that attenuation keeps constant at each wavelength, we can qualitatively benchmark both species penetration profiles at equivalent concentrations as these profiles shape is by definition constant (i.e. depths for a light decay to 1% of incident irradiance are exactly double than the corresponding to 10%). In other words, we perform a qualitative assessment to validate our results.

In Fig. 9 we can observe that the indirectly measured Spirulina penetration depths and WT Synechocystis calculated ones practically overlap each other. This shows that the model is also capable of predicting properties that have spectral resolution, such as wavelength dependent light attenuation. Moreover, as seen in the plot, Olive penetration depths are similar to WT ones within the whole PAR range with the remarkable exception of the red band, due to the previously mentioned phycobilisome absence. In this spectral region, Olive cultures allow an additional two centimetres of light penetration in comparison with WT in the given conditions.

Finally, we did calculate another optical property: the spectral photon flux density within the cultures taking into account the four lamps assessed in this contribution. Simulated environment inside the PBR was hypothesised for an average acclimation intensity of 80 $\mu mol\, photons \cdot m^{-2} \cdot s^{-1}$, at an incident exposure irradiance of 1,000 $\mu mol\, photons \cdot m^{-2} \cdot s^{-1}$ in a 4-cm deep PBR and with a suspension OD_{750} value of 1.0. The result is depicted in Fig. 10 at 0, 1 and 2 cm depth within the PBR.

The most interesting feature of such a spectral description of light is to gather information on the remaining irradiance at target wavelengths that can promote specific photosynthetic processes at a deeper depth. The differentiated effect of attenuation on specific wavelengths can be better appreciated in the white light example as green band photons are much less attenuated and they are the predominant colour at deeper distances.

3.5 Attenuation coefficient formula in Synechocystis cultures

Once the algorithm has been validated, simulations can be performed to estimate the PAR downward attenuation for both strain cultures given the incident irradiance, the length of the PBR and a constant cell density inside the reactor. As a representative example, attenuation coefficients for the studied range of cell densities and light intensities inside a PBR with a depth of 4 cm are shown in Fig. 11. It can be observed that the slope of attenuation coefficients is higher at lower chlorophyll concentration values. In these conditions, average irradiance inside the suspension drops quickly and as a result, the chlorophyll-specific attenuation $\overline{K}^{\star}_{d,\mathrm{PAR}}(E_{d,acc})$ does too (Fig. 6). Above concentration values of 10,000 $mg\ Chla \cdot m^{-3}$ average irradiance is kept low and practically constant, and similarly the chlorophyll-specific attenuation coefficient stays low, too. In this way, from a given chlorophyll amount, the resulting attenuation coefficient for downward irradiance increases linearly.

Finally, as a practical outcome of our investigation, our procedure delivers a simplified general estimation of PAR attenuation in different acclimatisation conditions for Synechocystis suspension within flat-type one side illuminated PBRs. For this purpose, the obtained data were correlated by an empirical equation:

$$\overline{K}_{d,\mathrm{PAR},WT} = \frac{17.9+0.0178\cdot\epsilon}{200+1049\cdot\delta} \cdot \rho^{0.8} \tag{14}$$

$$\overline{K}_{d,\mathrm{PAR},Olive} = \frac{13.7+0.0234\cdot\epsilon}{216+1938\cdot\delta} \cdot \rho^{0.8} \tag{15}$$

where ϵ represents the incident irradiance emitted by the lamp ($\mu mol\, photons \cdot m^{-2} \cdot s^{-1}$), δ stands for the depth of the photobioreactor (m) and ρ is the cell density expressed as the concentration of chlorophyll a in the suspension ($mg\ Chla \cdot m^{-3}$). The estimation of the downward attenuation coefficient, expressed in m^{-1}, is valid within the analysed range of average intensities, which accounts for roughly 10-100 $\mu mol\, photons \cdot m^{-2} \cdot s^{-1}$. For typical PBR depths and the already assessed cell-densities, this operation interval corresponds to 20-150 $\mu mol\, photons \cdot m^{-2} \cdot s^{-1}$ incident irradiance. The other variable ranges are 0.01-0.10 m for the PBR depth and 0-25,000 $mg\ Chla \cdot m^{-3}$ for the chl a concentration. Additionally, our IOPs spectra were obtained under a cool white light LED so the attenuation coefficients estimated here will likely not be the same when a light source with dissimilar spectral characteristics is employed.

4 Conclusions and future work

In this work, a new model to estimate downward light attenuation has been presented. The described methodology makes use of a semi-empirical correlation that was developed for marine biology applications. This, together with some simplifying assumptions of homogeneity, acclimation response of the cells and linearity of the Inherent Optical Properties, allows one to make predictions about the average field inside the PBR and the corresponding attenuation light profile. The proposed mathematical algorithm is based on the solution of a self-consistency problem, where the average irradiance depends on the downward attenuation coefficient and vice versa. Moreover, it can be applied to any type of PBR geometry, lamp arrangement and spectra, although in our work we have derived concrete expressions for the case of a flat-type PBR illuminated on just one side.

To check the validity of this approach, a combined analysis of experiments performed by the authors of this work together with the data obtained by Lea-Smith and co-workers was carried out on the same organisms, namely WT and Olive strains of Synechocystis .

Despite the different assumptions, we have benchmarked our predictions with experimental data to show that the model is able to reasonably predict light attenuation for both strains at various OD values and different colour LED light with a small support of additional assumptions. Thus, we conclude that it is possible to predict the light field inside PBRs operating under a broad range of conditions with a reduced set of previously-measured Inherent Optical Properties of the organism of interest. Moreover, knowing the exact acclimatisation intensity would allow a better prediction of the real attenuation profiles.

Our methodology opens further possibilities, e.g. to evaluate other illumination conditions and benchmark photosynthetic organisms, assessing possible improvements on the cultivation conditions and the PBR set-up. A further research line should cope with photo-adaptation and photo-inhibition dynamics, considering optical spectra changes upon radiation variations. In this regard, to leverage in silico absorption coefficient estimations in terms of light quality and quantity changes, further information on pigment concentration is desired. Additionally, this model can be coupled to others describing the production of oxygen or other compounds, allowing an improvement of their prediction capacity.

In summary, it is getting more common to study the light impact on photosynthesis, not just for optimising large-scale photobioreactor operation but also to better understand the underlying mechanisms that trigger optically-dependent processes that control photosynthesis, and therefore metabolism, indirectly. In this regard, our approach aims to be the first step towards a more integrative modelling of optical properties inside PBR cultures and to better understand the challenge of describing the effect of light on photosynthetic microorganisms.

5 Acknowledgements

This project has received funding from the European Union?s Seventh Programme for research, technological development and demonstration under grant agreement No 308518 CyanoFactory, to Javier Urchueguía's and Matthias Rögner's respective research groups and from the grant Contratos Predoctorales FPI 2013 of the Universitat Politècnica de València to the first one. We would also like to thank David Lea-Smith and Dariusz Stramski for their fruitful and selfless contribution. We kindly acknowledge the experimental support of Saori Fuse for the cultivation of

cyanobacteria.

Name	Definition	Unit
PAR	Photosynthetically Active Radiation are those wavelengths in the range between 400 nm and 700 nm	
G	A coefficient representing the relative contribution of scattering to vertical attenuation	
$\cos\varphi_0$	Cosine of the angle of the photons to the vertical just below the water surface after refraction	
$\rho_{Chl\ a}$	Chlorophyll a concentration in the culture	$mg\ Chla \cdot m^{-3}$
OD_X	Optical density at given wavelength x in nm	
$\Phi_a(\lambda)$, $\Phi_b(\lambda)$, $\Phi_c(\lambda)$ $\Phi_t(\lambda)$, $\Phi_i(\lambda)$	Radiant flux absorbed, scattered, attenuated, transmitted and incident	W
IOPs	Inherent Optical Properties of the culture components	
$a(\lambda)$	Absorption coefficient	m^{-1}
$b(\lambda)$	Total scattering coefficient	m^{-1}
$c(\lambda)$	Beam attenuation coefficient	m^{-1}
att	Attenuance defined as the negative common logarithm of the transmittance	
opd	Absorbance defined as the negative common logarithm of the transmittance in the absence of scattering	
$j^\star(\lambda, E_{d,acc})$	$\rho_{Chl\ a}$ specific coefficient at wavelength λ and where culture is acclimated at intensity $E_{d,acc}$; j is a placeholder that either stands for a, b or c	$m^2 \cdot mg\ Chla^{-1}$
AOPs	Apparent Optical Properties of a PBR culture in a given photo-physiological context	
$E_d(\lambda, z)$	Downward irradiance at the depth z and at wavelength λ	$\mu mol\, photons \cdot m^{-2}$
$E_{d,\text{PAR}}(z)$	Downward irradiance integrated over PAR and at the depth z	$\mu mol\, photons \cdot m^{-2}$
$\rho E_d(\lambda, z)$	Spectral photon flux density of downward irradiance at the wavelength λ and depth z	$\mu mol\, photons \cdot m^{-2}$
$E_{d,\text{acc}}$	Volume averaged and PAR integrated downward irradiance to which a given PBR culture has been acclimated	$\mu mol\, photons \cdot m^{-2}$
$K_d(\lambda, z)$	Downward attenuation coefficient at the depth z and at wavelength λ	m^{-1}
$\overline{K}_d(\lambda, E_{d,acc})$	Mean downward attenuation coefficient at wavelength λ averaged for a culture acclimated at intensity $E_{d,acc}$	m^{-1}
$\overline{K}_{d,\text{PAR}}(E_{d,acc})$	Mean downward attenuation coefficient averaged within PAR range for a culture acclimated at intensity $E_{d,acc}$	m^{-1}
$\overline{K}^\star_{d,\text{PAR}}(E_{d,acc})$	Chlorophyll a-specific mean downward attenuation coefficient averaged within PAR range for a culture acclimated at intensity $E_{d,acc}$	$m^2 \cdot mg\ Chla^{-1}$

Table 1: List of symbols and abbreviations.

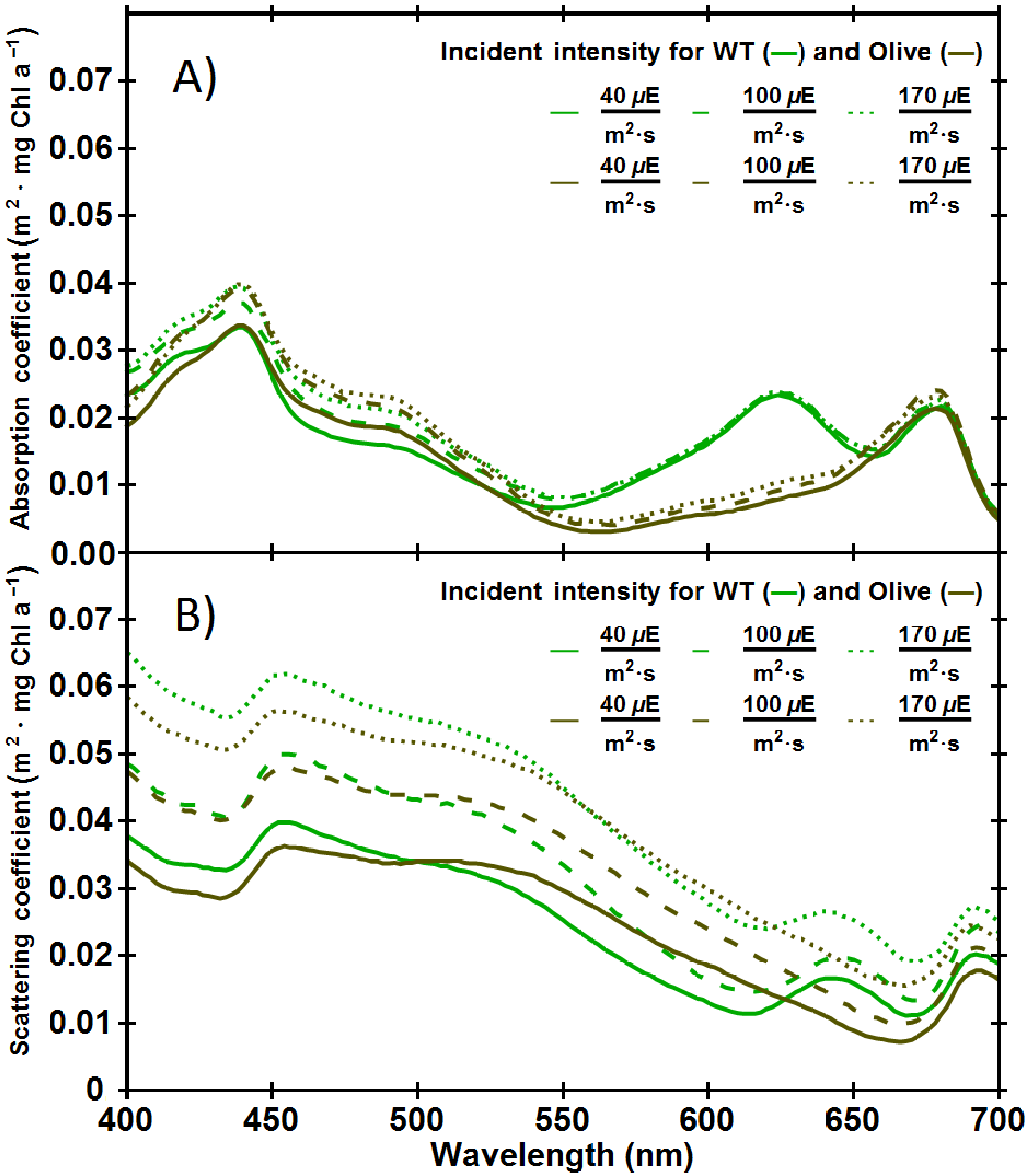

Figure 4: (A) Absorption $a^{\star}(\lambda, E_{d,i})$ and (B) total scattering $b^{\star}(\lambda, E_{d,i})$ chl a-specific coefficients within PAR waveband of wild-type and Olive strain (green and brown colour, respectively) grown at incident light intensities of 40, 100 (dashed) and 170 (dotted) $\mu mol\, photons \cdot m^{-2} \cdot s^{-1}$ in a 4-cm flat-type photobioreactor.

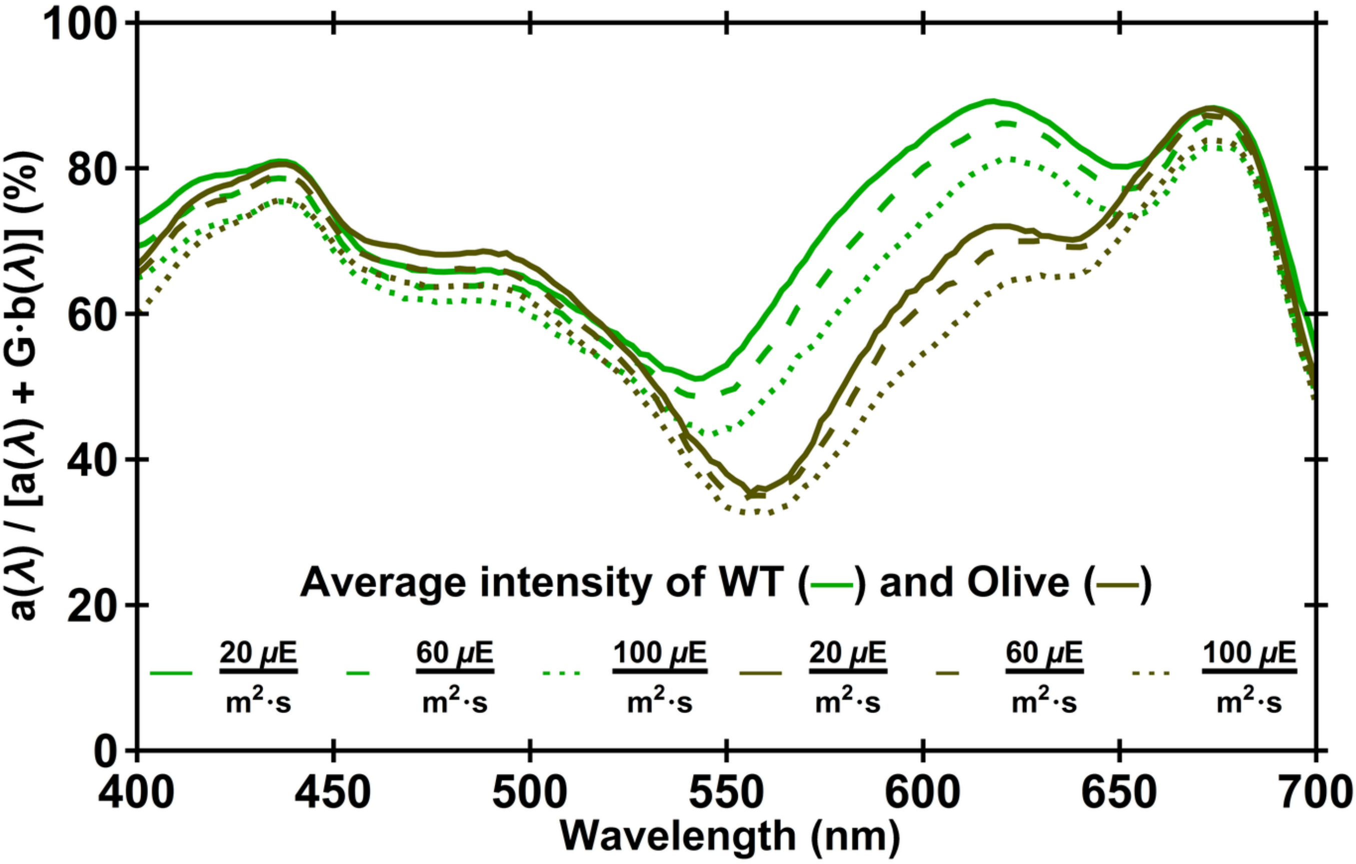

Figure 5: Modelled photon absorption contribution of wild-type and Olive strain (green and brown colour, respectively) grown at average light intensities of 20, 60 (dashed) and 100 (dotted) $\mu mol\, photons \cdot m^{-2} \cdot s^{-1}$ for each wavelength within PAR range following Kirk's formula.

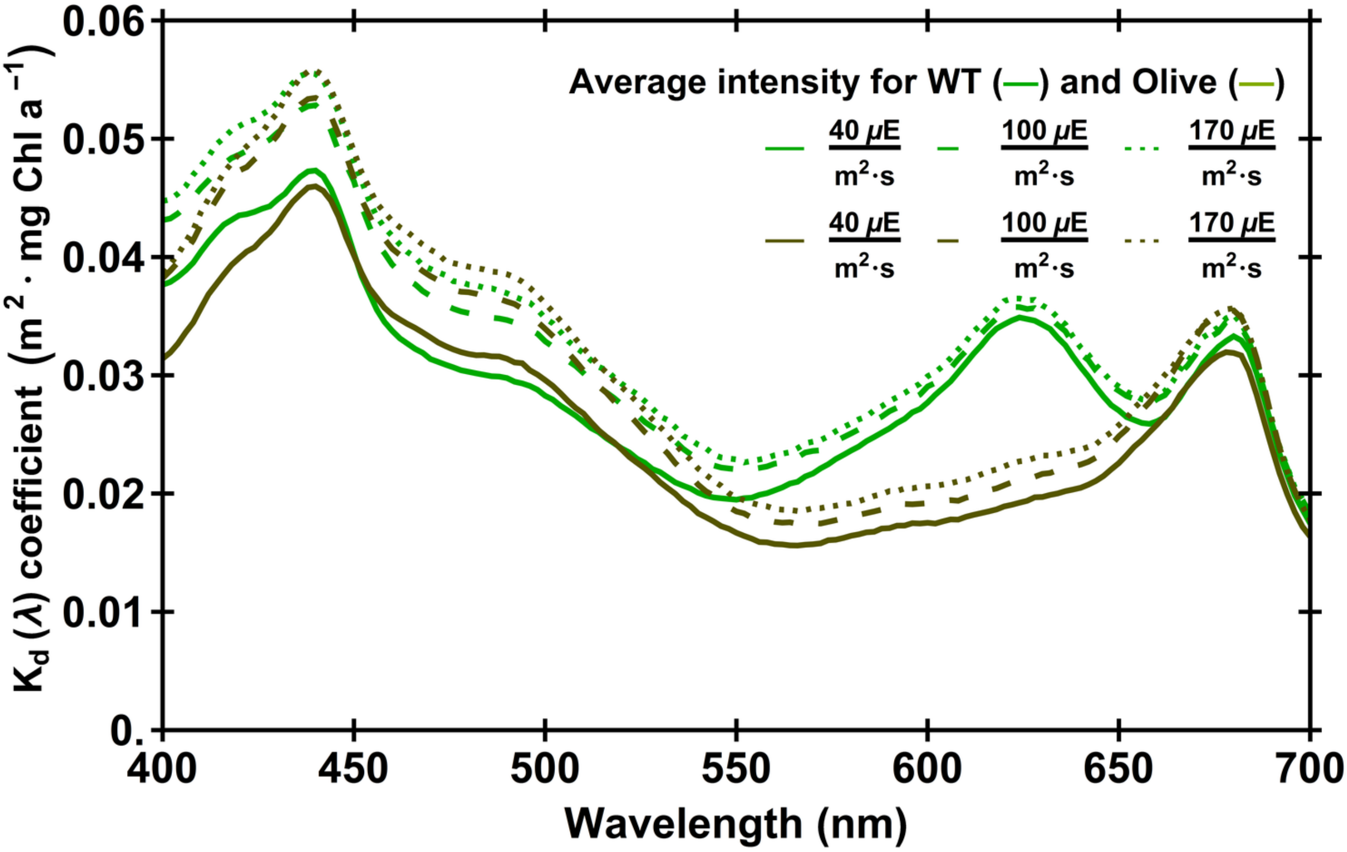

Figure 6: Modelled chlorophyll-specific downward attenuation function $\overline{K}_d^\star(\lambda, E_{d,i})$ for wild-type and Olive strain (green and brown colour, respectively) at the incident irradiance values of 40, 100 (dashed) and 170 (dotted) $\mu mol\, photons \cdot m^{-2} \cdot s^{-1}$.

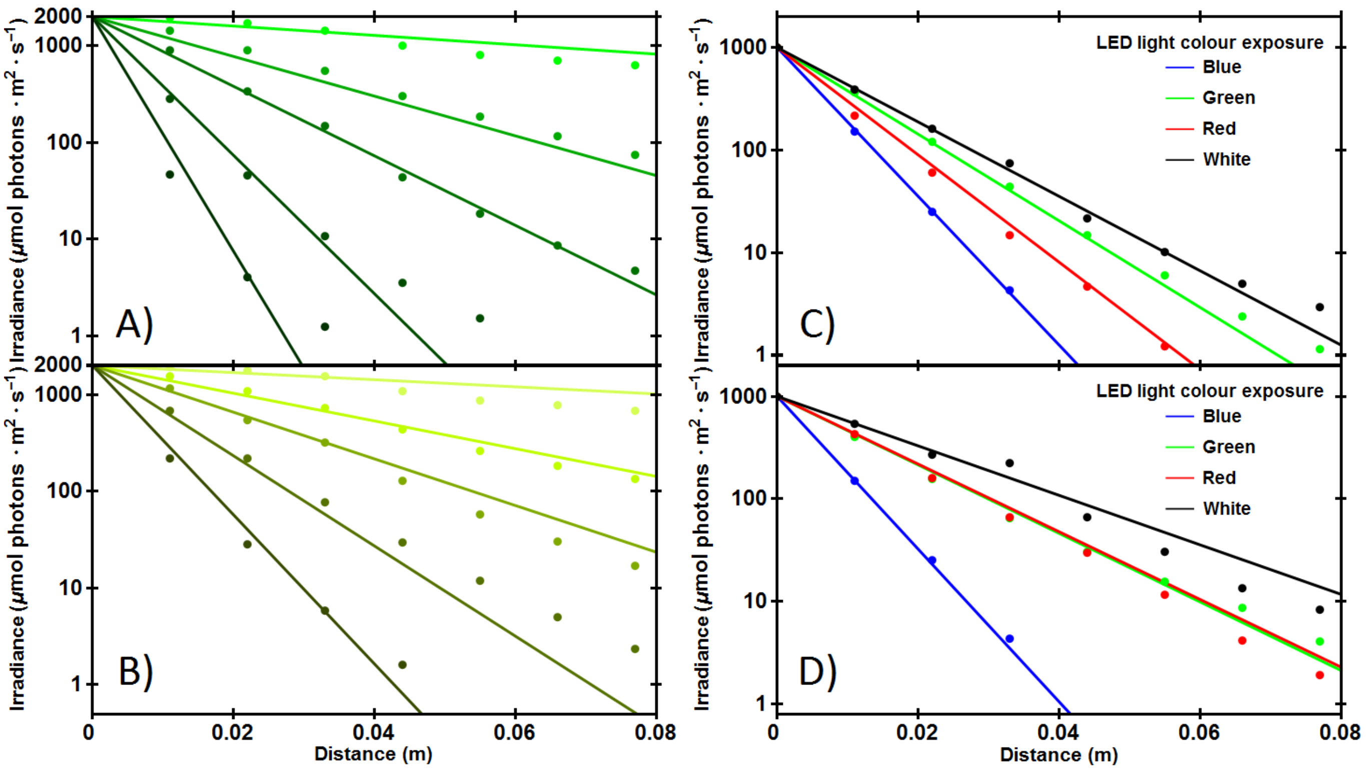

Figure 7: Left panel: Light attenuation profiles of Synechocystis WT (A) and Olive (B) strain cultures exposed to 2000 $\mu mol\, photons \cdot m^{-2} \cdot s^{-1}$ of white LED light at five different OD_{750} concentrations (0.1, 0.5, 1.0, 2.5 and 5.0) are depicted. Dots are the original source samples [38] and lines the simulation outcome. Darker colours correspond to denser suspensions. Right panel: Light attenuation profiles of Synechocystis WT (C) and Olive (D) strain cultures exposed to 1000 $\mu mol\, photons \cdot m^{-2} \cdot s^{-1}$ of four different LED lamps at an OD_{750} concentration of 1.0 are shown. Dots are the original source samples. Graph colours represent each LED characteristic colour (blue, green and red), whereas black curve corresponds to the white LED.

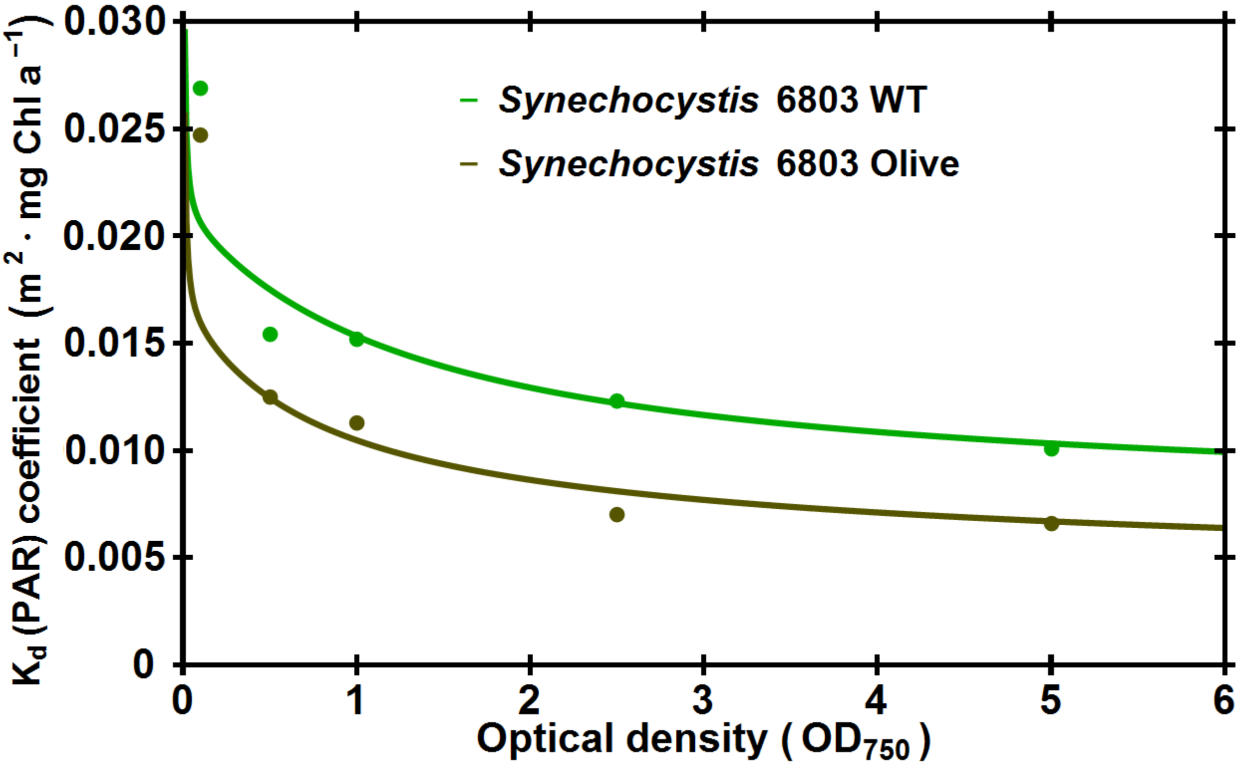

Figure 8: Chlorophyll a-specific mean downward attenuation coefficient $\overline{K}^{\star}_{d,\mathrm{PAR}}(E_{d,acc})$ comparison for WT and Olive strains (green and brown colour, respectively) between experimental (dots) and modelled values at the given densities. Experimental coefficients were obtained from the white lamp exposure assays at 2,000 $\mu mol\, photons \cdot m^{-2} \cdot s^{-1}$ and calculated as irradiance-weighted attenuation coefficients, whereas the in silico values were directly obtained by dividing by the chlorophyll amount for each optical density.

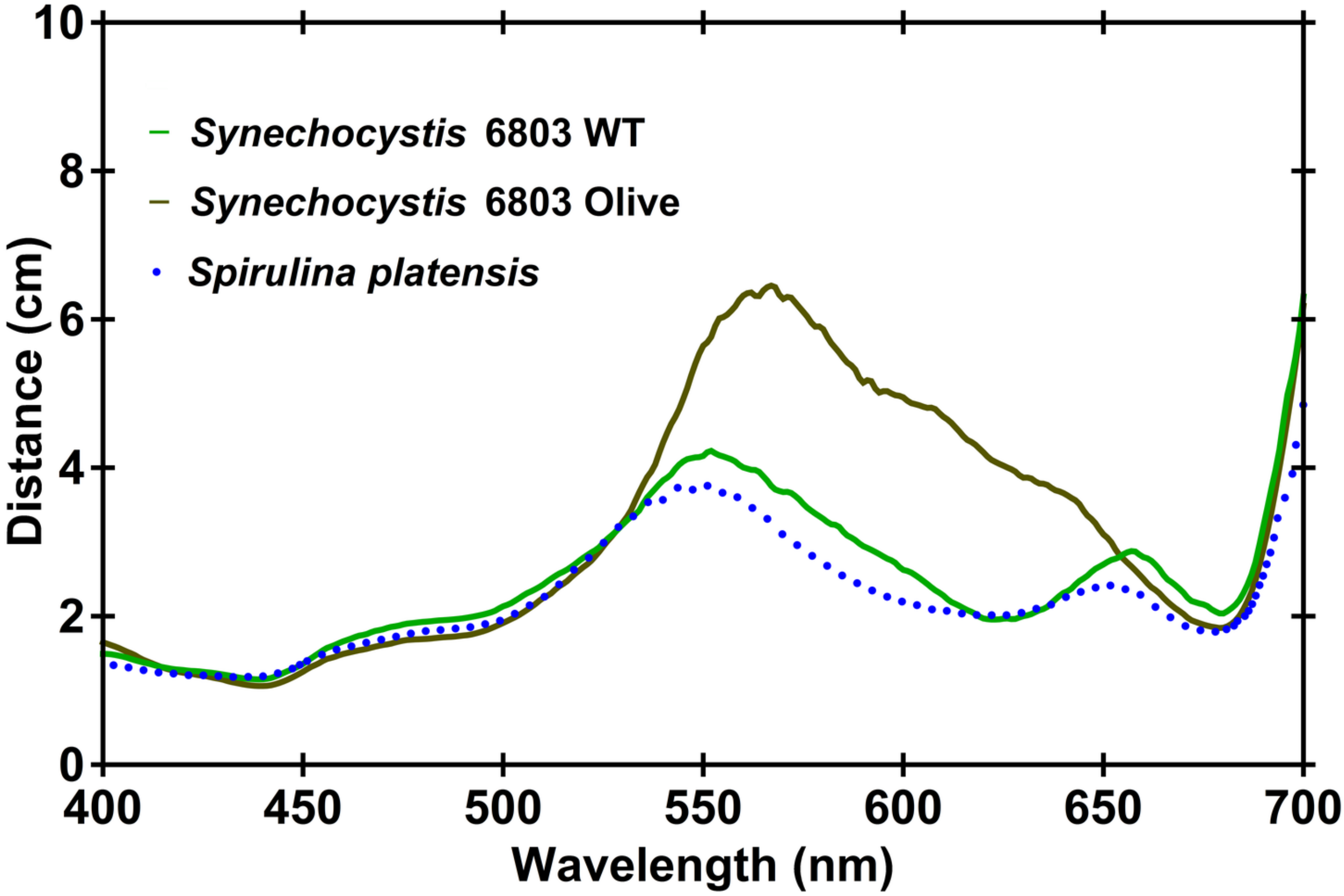

Figure 9: Penetration depth at which irradiance drops to 10 % of the initial value at each wavelength within PAR range for WT and Olive strains (green and brown colour, respectively). Simulation conditions correspond to Synechocystis WT cultures grown at typical PBR densities, i.e. 1.0 OD_{750}, and acclimatised to a lamp irradiance of 80 $\mu mol\, photons \cdot m^{-2} \cdot s^{-1}$ of white light. Blue dots correspond to Spirulina platensis depths estimated from experimental attenuation coefficients.

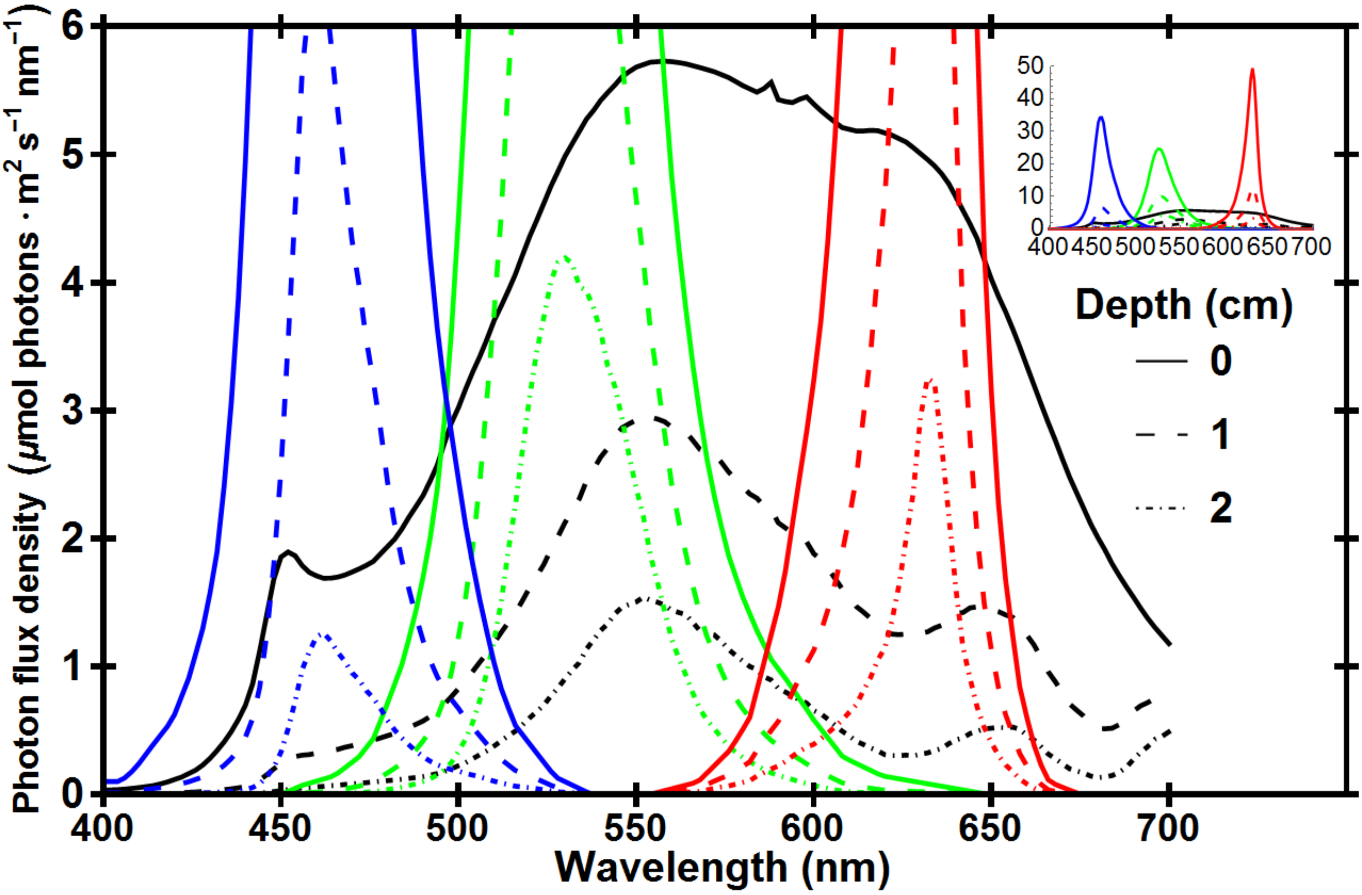

Figure 10: Modelled spectral photon flux densities $\rho E_d(\lambda, z)$ within simulated Synechocystis WT strain cultures are depicted, where cells are adapted to white light of 80 $\mu mol\, photons \cdot m^{-2} \cdot s^{-1}$ but momentarily exposed to 1,000 $\mu mol\, photons \cdot m^{-2} \cdot s^{-1}$ of different colour LED lamps (white, blue, green or red light) at an OD_{750} concentration of 1.0. Remaining photon flux densities at 0, 1 (dashed) and 2 cm (dotted) are shown. Inset plot shows whole graphs with the same units in both axes.

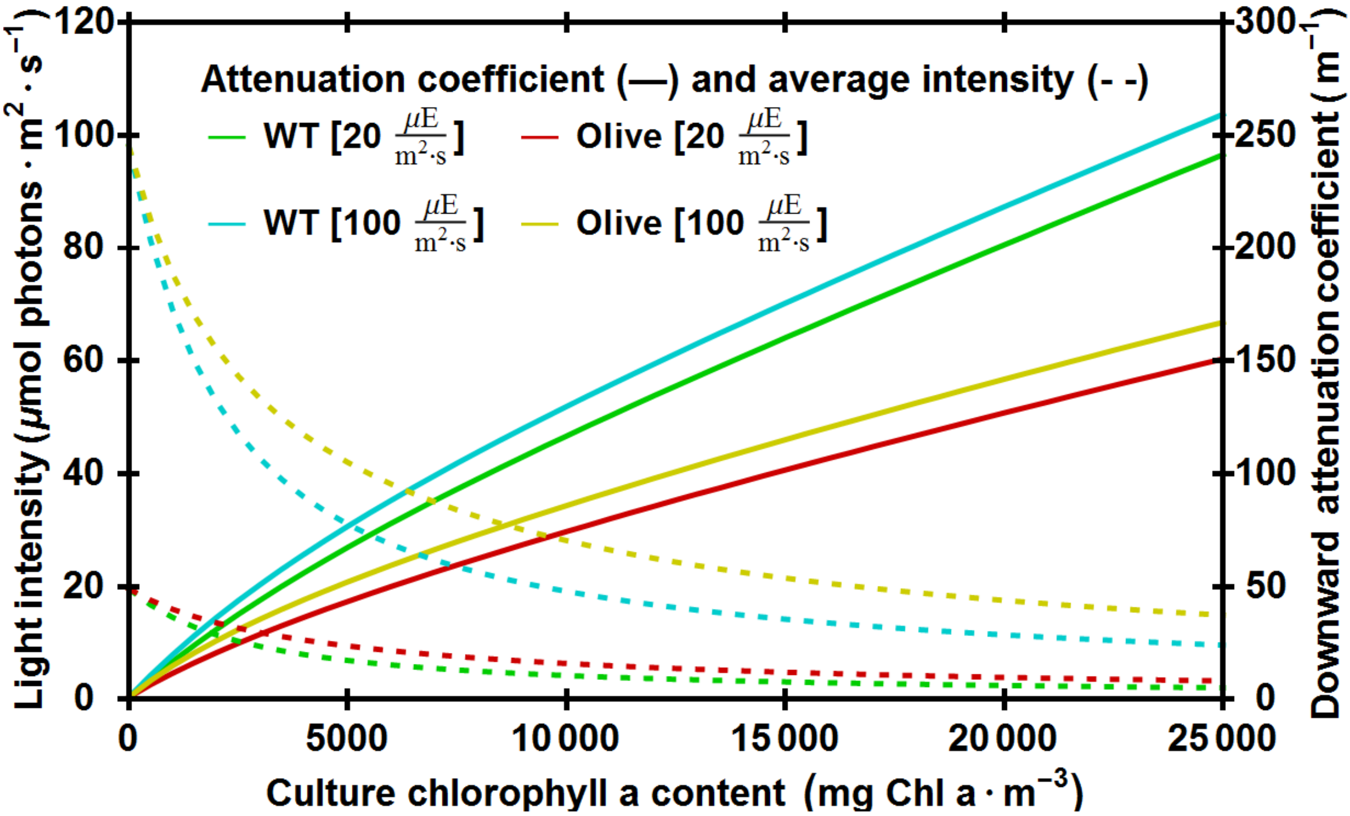

Figure 11: Modelled mean downward attenuation coefficient within PAR range $\overline{K}_{d,\mathrm{PAR}}(E_{d,acc})$ for WT cultures exposed to lamp intensities of 20 and 100 $\mu mol\, photons \cdot m^{-2} \cdot s^{-1}$ in a 4-cm depth PBR at constant cell-densities up to 25,000 $mg\ Chla \cdot m^{-3}$ are depicted (right vertical axis). Additionally, resulting average irradiance $E_{d,acc}$ is also plotted for such suspensions (dotted, left vertical axis). Green and blue curves stand for WT cultures grown at 20 and 100 $\mu mol\, photons \cdot m^{-2} \cdot s^{-1}$ incident radiation and similarly red and yellow curves represent Olive cultures cultivated at 20 and 100 $\mu mol\, photons \cdot m^{-2} \cdot s^{-1}$ incident radiation.

References

[1] R W Preisendorfer. Application of radiative transfer theory to light measurements in the sea. International Union of Geodesy and Geophysics monograph, 10:11–30, 1961.

[2] D Antoine, M Babin, J F Berthon, A Bricaud, B Gentili, H Loisel, S Maritorena, and D Stramski. Shedding light on the sea: André morel's legacy to optical oceanography. Annual Review of Marine Science, 6:1–21, 2014.

[3] A Morel. Light and marine photosynthesis: a spectral model with geochemical and climatological implications. Progress in Oceanography, 26:263–306, 1991.

[4] Eleftherios Touloupakis, Ana Margarita Silva Benavides, Bernardo Cicchi, and Giuseppe Torzillo. Growth and hydrogen production of outdoor cultures of synechocystis pcc 6803. Algal Research, 18:78 – 85, 2016.

[5] Yusuf Chisti. Biodiesel from microalgae. Biotechnology Advances, 25(3):294 – 306, 2007.

[6] Amos Richmond. Growth characteristics of ultrahigh-density microalgal cultures. Biotechnology and Bioprocess Engineering, 8(6):349–353, 2003.

[7] Niels-Henrik Norsker, Maria J Barbosa, Marian H Vermuë, and René H Wijffels. Microalgal production—a close look at the economics. Biotechnology Advances, 29(1):24–27, 2011.

[8] A Gitelson, Q Hu, and A Richmond. Photic volume in photobioreactors supporting ultrahigh population densities of the photoautotroph spirulina platensis. Applied and Environmental Microbiology, 62:1570–1573, 1996.

[9] C Posten. Design principles of photo-bioreactors for cultivation of microalgae. Engineering in Life Sciences, 9:165–177, 2009.

[10] Ziauddin Ahmad and Robert S Fraser. An iterative radiative transfer code for ocean-atmosphere systems. Journal of the Atmospheric Sciences, 39(3):656–665, 1982.

[11] J T O Kirk. A monte carlo study of the nature of the underwater light field in, and the relationships between optical properties of, turbid yellow waters. Australian Journal of Marine and Freshwater Research, 32:517—-532, 1981.

[12] Jérémi Dauchet, Stéphane Blanco, Jean-François Cornet, Mouna El Hafi, Vincent Eymet, and Richard Fournier. The practice of recent radiative transfer monte carlo advances and its contribution to the field of microorganisms cultivation in photobioreactors. Journal of Quantitative Spectroscopy and Radiative Transfer, 128:52–59, 2013.

[13] Ignacio Niizawa, Josué Miguel Heinrich, and Horacio Antonio Irazoqui. Modeling of the influence of light quality on the growth of microalgae in a laboratory scale photo-bio-reactor irradiated by arrangements of blue and red leds. Biochemical Engineering Journal, 90:214–223, 2014.

[14] Ward Blanken, P Richard Postma, Lenneke de Winter, René H Wijffels, and Marcel Janssen. Predicting microalgae growth. Algal Research, 14:28–38, 2016.

[15] JF Cornet, CG Dussap, and G Dubertret. A structured model for simulation of cultures of the cyanobacterium spirulina platensis in photobioreactors: I. coupling between light transfer and growth kinetics. Biotechnology and Bioengineering, 40(7):817–825, 1992.

[16] L Pottier, Jérémy Pruvost, J Deremetz, J-F Cornet, Jack Legrand, and CG Dussap. A fully predictive model for one-dimensional light attenuation by chlamydomonas reinhardtii in a torus photobioreactor. Biotechnology and bioengineering, 91(5):569–582, 2005.

[17] Josué Miguel Heinrich, Ignacio Niizawa, Fausto Adrián Botta, Alejandro Raúl Trombert, and Horacio Antonio Irazoqui. Analysis and design of photobioreactors for microalgae production ii: experimental validation of a radiation field simulator based on a monte carlo algorithm. Photochemistry and photobiology, 88(4):952–960, 2012.

[18] M Rögner, Peter J Nixon, and Bruce A Diner. Purification and characterization of photosystem i and photosystem ii core complexes from wild-type and phycocyanin-deficient strains of the cyanobacterium synechocystis pcc 6803. Journal of Biological Chemistry, 265(11):6189–6196, 1990.

[19] A Morel. Chlorophyll-specific scattering coefficient of phytoplankton. a simplified theoretical approach. Deep Sea Research Part I: Oceanographic Research Papers, 34:1093–1105, 1987.

[20] M Brody and R Emerson. The effect of wavelength intensity of light on the proportion of pigments in porphyridium cruentum. American Journal of Botany, 46:433–440, 1959.

[21] DC Fork. Observations of the function of chlorophyll a and accessory pigments in photosynthesis. Photosynthesis Mechanisms in Green Plants. National Academy of Science-National Research Council, pages 352–361, 1963.

[22] F García-Camacho, A Sánchez-Mirón, E Molina-Grima, F Camacho-Rubio, and JC Merchuck. A mechanistic model of photosynthesis in microalgae including photoacclimation dynamics. Journal of theoretical biology, 304:1–15, 2012.

[23] W Ma, T Ogawa, Y Shen, and H Mi. Changes in cyclic and respiratory electron transport by the movement of phycobilisomes in the cyanobacterium synechocystis sp. strain pcc 6803. Biochimica et Biophysica Acta (BBA)-Bioenergetics, 1767:742–749, 2007.

[24] R M Schuurmans, J M Schuurmans, M Bekker, J C Kromkamp, H C Matthijs, and K J Hellingwerf. The redox potential of the plastoquinone pool of the cyanobacterium synechocystis species strain pcc 6803 is under strict homeostatic control. Plant physiology, 165:463–475, 2014.

[25] T Zavřel, M A Sinetova, D Búzová, P Literáková, and J Červený. Characterization of a model cyanobacterium synechocystis sp. pcc 6803 autotrophic growth in a flat-panel photobioreactor. Engineering in Life Sciences, 15:122–132, 2015.

[26] G Markou. Effect of various colors of light-emitting diodes (leds) on the biomass composition of arthrospira platensis cultivated in semi-continuous mode. Applied Biochemistry and Biotechnology, 172:2758–2768, 2014.

[27] Tim de Mooij, Guus de Vries, Christos Latsos, René H Wijffels, and Marcel Janssen. Impact of light color on photobioreactor productivity. Algal Research, 15:32–42, 2016.

[28] D Stramski and A Morel. Optical properties of photosynthetic picoplankton in different physiological states as affected by growth irradiance. Deep Sea Research Part I: Oceanographic Research Papers, 37:245–266, 1990.

[29] J T O Kirk. Light and photosynthesis in aquatic ecosystems. Cambridge UK, Cambridge University Press, 1994.

[30] B B Jorgensen, Y Cohen, and D J Des Marais. Photosynthetic action spectra and adaptation to spectral light distribution in a benthic cyanobacterial mat. Applied and Environmental Microbiology, 53:879–886, 1987.

[31] RJ Davies-Colley, RD Pridmore, and JE Hewitt. Optical properties of some freshwater phytoplanktonic algae. Hydrobiologia, 133(2):165–178, 1986.

[32] John TO Kirk. The vertical attenuation of irradiance as a function of the optical properties of the water. Limnology and Oceanography, 48(1; NUMB 1):9–17, 2003.

[33] J T O Kirk. Attenuation of solar radiation in scattering-absorbing waters: a simplified procedure for its calculation. Applied Optics, 23:3737–3739, 1984.

[34] J-H Kwon, M Rögner, and S Rexroth. Direct approach for bioprocess optimization in a continuous flat-bed photobioreactor system. Journal of Biotechnology, 162:156–162, 2012.

[35] A E Rabe and R J Benoit. Mean light intensity—a useful concept in correlating growth rates of dense cultures of microalgae. Biotechnology and Bioengineering, 4:377–390, 1962.

[36] E Molina Grima, F García Camacho, J A Sánchez Pérez, J M Fernández Sevilla, F G Acién Fernández, and A Contreras Gómez. A mathematical model of microalgal growth in light-limited chemostat culture. Journal of Chemical Technology and Biotechnology, 61:167–173, 1994.

[37] E Molina Grima, F G Acién Fernández, F García Camacho, and Y Chisti. Photobioreactors: light regime, mass transfer, and scaleup. Journal of Biotechnology, 70:231–247, 1999.

[38] D J Lea-Smith, P Bombelli, J S Dennis, S A Scott, A G Smith, and C J Howe. Phycobilisome-deficient strains of synechocystis sp. pcc 6803 have reduced size and require carbon-limiting conditions to exhibit enhanced productivity. Plant Physiology, 165:705–714, 2014.

[39] H C Van de Hulst. Light scattering by small particles. John Wiley, 1957.

[40] W Zhang, Y Ren, Y Zhang, and Z Zhang. Light attenuation of synechocystis sp. pcc 6803 in photo-bioreactor and its growth dynamics research. Journal of Anhui Agricultural Sciences, 38:9957–9958,9967, 2010.

[41] Y-S Yun and J Park. Attenuation of monochromatic and polychromatic lights in chlorella vulgaris suspensions. Applied microbiology and biotechnology, 55:765–770, 2001.

[42] J-H Kwon, G Bernát, H Wagner, M Rögner, and S Rexroth. Reduced light-harvesting antenna: Consequences on cyanobacterial metabolism and photosynthetic productivity. Algal Research, 2:188–195, 2013.

[43] S G H Simi and H M Kauko. In vivo mass-specific absorption spectra of phycobilipigments through selective bleaching. Limnology and Oceanography: Methods, 10:214–226, 2012.

[44] A Morel and A Bricaud. Theoretical results concerning the optics of phytoplankton, with special reference to remote sensing applications. In Oceanography from space, pages 313–327. Springer, 1981.